

# $\Lambda$ -Neutron Scattering Lengths from Radiative $K^-$ Capture

W. R. Gibbs, S. A. Coon, H. K. Han

Department of Physics, New Mexico State University, Las Cruces, NM, 88003

B. F. Gibson

Theoretical Division, Los Alamos National Laboratory, Los Alamos, NM, 87545

February 8, 2008

## Abstract

Radiative capture of the  $K^-$  by the deuteron is examined as a reaction for measurement of the  $\Lambda$ -neutron scattering lengths. Using the final state interaction, analogous to measurements of the radiative capture of pions by deuterium, the scattering lengths of both the triplet and singlet  $\Lambda$ -n interaction can be inferred. The problem of the separation of these two fundamental parameters without and with spin information in the experiment is addressed. It is shown that a measurement of the deviation of the vector deuteron polarization asymmetry from  $-1$  provides a direct determination of the difference of the singlet and triplet scattering lengths.

# 1 Introduction

The interaction of the nucleon with the  $\Lambda$  hyperon is of great theoretical interest. Since the one-pion-exchange interaction is absent (except under broken isospin [1]), one is able to focus on the shorter range contributions to the interaction. The singlet and triplet scattering lengths are predicted to be equal by  $SU(6)$  symmetry.

Unfortunately, experiments are difficult to perform for this system because of the short lifetime of the  $\Lambda$ . Nevertheless, some experimental results do exist[2] and have been analyzed[3, 4]. Rijken *et al.*[3] have recently generated a set of potentials which fit these data. The range of scattering lengths obtained from this analysis is rather large, which is perhaps a natural consequence considering that the data do not extend to low energies.

Use of the radiative capture of a  $\pi^-$  from an s-wave atomic state by deuterium to measure the neutron-neutron (nn) scattering length, through the influence of the final state interaction, was investigated in an experiment by Phillips and Crowe[5] and soon after studied theoretically by McVoy[6] and Bander[7]. The basic technique consists of comparing the shape of the photon spectrum with calculations. Because of the final-state interaction of the two neutrons, a peak results near the high-energy end of the spectrum corresponding to a maximum in the s-wave phase shifts at low neutron-neutron energy. Since this phase shift rises very quickly to a maximum, as a function of energy in the neutron-neutron frame, the peak in the photon spectrum is very near the maximum energy. It is also possible to use the neutron spectrum at low energies for the studies provided that the angle between the neutron and photon is known. Experiments have been performed in both geometries.

These early exploratory efforts were followed by an experiment detecting the neutrons[8] which gave useful results. Following a study of limits due to the theoretical uncertainties[9], experiments were carried out at the Paul Scherrer Institute (PSI) detecting only the photon, as well as experiments in which the photon and neutron were detected in coincidence[10]. These experiments resulted in values for the nn scattering length (and effective range) which were considered to be the best obtained to date. Recently another experiment was performed using this reaction at the Clinton P. Anderson Meson Physics Facility[11]. Results from this experiment appear to confirm the PSI results. The uncertainty in the scattering length is of the order of  $\pm 0.5$  fm for a value of -18.58 fm, about 2-3%.

A determination of the  $\Lambda n$  scattering lengths from the photon spectrum of the reaction  $K^- d \rightarrow n \Lambda \gamma$ , where the capture takes place from an atomic state, was suggested by Gibson *et al.*[12]. A study of this process performed by Workman and Fearing [13] concluded that the different hadronic routes considered by Akhiezer *et al.*[14] had a negligible impact on a possible measurement (however, see Refs. [15] for comments on their representation of the amplitudes). They also concluded that the dominant operator for the conversion of a proton to a  $\Lambda$  through radiative capture of a kaon was of the Kroll-Ruderman form

$$\mathcal{O} = \boldsymbol{\sigma} \cdot \boldsymbol{\epsilon} \quad (1)$$

where  $\boldsymbol{\epsilon}$  is the polarization of the outgoing photon and  $\boldsymbol{\sigma}$  is the spin operator for the proton on which the capture takes place.

At the same time as this theoretical effort, a feasibility study[16] demonstrated that the spectrum for this reaction could be separated from the background. Workman and Fearing compared their analysis with these data to show that reasonable values of the scattering lengths were consistent with the data.

Two important issues were left unresolved by the work of Workman and Fearing. They used only the asymptotic  $\Lambda$ -neutron wave functions. In the work of Ref. [9] the lack of knowledge of the short range final-state wave function was found to be the dominant theoretical uncertainty in the analysis of the scattering length, of the order of  $\pm 0.3$  fm. If the uncertainty is of the same order in the case of  $\Lambda$ -neutron scattering the consequences are more serious since the scattering length itself is thought to be an order of magnitude smaller.

A second problem, which may be more serious, is that, while in the case of the neutron-neutron final state the spin state of the two neutrons is restricted to be singlet by the Pauli principle, the  $\Lambda n$  final state consists of a mixture of a singlet and triplet states. One expects that the scattering in these two states may be different, and indeed the dependence of the scattering length on the spin might provide some very important clues to the structure of the interaction. While it has been suspected that polarization information may provide a tool to obtain a singlet-triplet separation (see Balewski *et al.*[17] for example), we provide here the formalism and expressions necessary to obtain such a separation for this reaction.

We first give a brief heuristic description of the basic physics underlying the development to follow. Consider a deuteron target prepared in a configuration with only magnetic spin projection zero along a z-axis defined by the direction of the photon. Assume also that the final state of the  $\Lambda$ -n system is in a singlet state. Since the  $K^-$  is assumed to be captured from an atomic s-state, there will be a total spin projection of zero in the initial state and zero angular momentum projection in the final state, other than that due to the spin of the  $\gamma$ . Since the “transversality” relation,

$$\boldsymbol{\epsilon} \cdot \mathbf{k} = 0, \quad (2)$$

requires that the spin projection of the photon must lie along its direction of travel (i.e. there is no zero spin projection) this assumed transition to the singlet final state must have zero amplitude due to the conservation of the z-projection of angular momentum. Thus, for example, a spectrum taken under these conditions could be analyzed to obtain the triplet scattering parameters alone.

The previous paragraph gives only an example of how deuteron spin information can affect the analysis. A measurement of the photon circular polarization can also help to separate the singlet and triplet scattering states. In the subsequent sections

we develop the expressions necessary to calculate the photon spectrum and provide specific results.

## 2 Expressions for the Rate

For comparison with the measurement we need the theoretical prediction for the shape of the spectrum. The absolute rate is not usually measured in this type of experiment.

### 2.1 Kinematics and Phase Space

The magnitude of the momentum,  $\mathbf{p}$ , of each baryon in this pair's center of mass is given by

$$p^2 = \frac{(s + M_n^2 - M_\Lambda^2)^2}{4s} - M_n^2 \quad (3)$$

with  $s$  the center of mass energy of the  $\Lambda$ -neutron pair given by

$$s = E_0^2 - 2kE_0, \quad (4)$$

where  $E_0$  is the total energy of the initial system and  $k$  is the final photon momentum.  $M_\Lambda$  and  $M_n$  are the masses of the  $\Lambda$  and neutron respectively.

Since we shall assume that the final-state baryons are not observed, we must integrate over their directions, giving for the differential rate of the observed photon

$$\frac{d\Gamma}{d\Omega_{\mathbf{k}}dk} \propto \frac{pk\omega_\Lambda\omega_n}{(\omega_\Lambda + \omega_n)} \int |M|^2 d\Omega_{\mathbf{p}} \quad (5)$$

The total energies,  $\omega_n$  and  $\omega_\Lambda$  are very nearly constant over the energy range of interest.

It should be noted that a single factor of the photon momentum  $k$  appears. It is linear only with relativistic phase space; it would appear to the second power in non-relativistic phase space. When this reaction was first proposed, the non-relativistic version was usually used (in fact Williams [18] used this reaction as an example of the use of non-relativistic phase space). Of course, either type of phase space can be used provided that the proper corresponding operator is used. The difference between a first and second power of the photon momentum is relativistic in origin and the effect is very small in many cases. In the analysis of Ref. [10] only the very end of the spectrum was used and the photon momentum is sufficiently constant over this range that such a factor is immaterial. For the analysis of Ref. [11] the larger range of the spectrum used leads to a small sensitivity to the power of  $k$  used in this expression. For the present reaction, since the peak lies farther from the end point of the spectrum than for the  $\pi^-d \rightarrow nn\gamma$  reaction, a larger range of photon momenta may be included in the analysis and the correct factor is more important.

## 2.2 Matrix Element

The mathematical development of the expressions for the matrix element used here follows a different procedure than that of Refs. [9] and [13]. The previous methods have written the matrix element for the transition first as a plane wave transition then corrected this expression by adding and subtracting the s-wave contribution. The s-wave contribution with a final state interaction is then substituted in the added element. For a matrix element with two particles detected in the final state this is the appropriate method. However, for the case in which only the photon is detected, there is an average over the unobserved baryon momenta which must be made as outlined in the previous section. This integral was carried out numerically in the previous developments.

In the method used in the present analysis the partial-wave quantities are calculated in terms of the relative  $\Lambda$ -neutron momentum. This technique requires several partial waves to be computed for a handful of magnetic quantum numbers. While it may seem *a priori* less efficient, in the end it has several advantages. The first is that the final averaging over the direction of the unobserved momenta can be done analytically. Since the contributions from the higher partial waves depend only on the initial state wave functions (we assume no interaction in partial waves higher than  $\ell = 0$ ), if one wishes to fit the data by varying the scattering length and effective range for the singlet and triplet states, these higher partial waves need be calculated only once.

A second advantage is that the degree of coherence or incoherence of the singlet and triplet states is manifest. For example, we will see that if all magnetic quantum numbers of the initial deuteron are equally populated and the polarization of the final photon is not observed, the transitions to the singlet and triplet final states are incoherent.

The matrix element for the reaction which proceeds from an initial deuteron with spin-projection  $S_z$  to a final state of the  $\Lambda$ -neutron system in a total spin state  $(S', S'_z)$  is

$$M^{S', S'_z, S_z} = \int d\mathbf{r}_1 d\mathbf{r}_2 \langle S' S'_z | \psi_{S'}^-(\mathbf{p}, \mathbf{r}) e^{-i\mathbf{K} \cdot (\mathbf{r}_1 + \mathbf{r}_2)} | \mathcal{O} e^{i\mathbf{k} \cdot \mathbf{r}_1} | \Psi_D^{S_z}(\mathbf{r}) \rangle \quad (6)$$

where  $\psi_{S'}^-(\mathbf{p}, \mathbf{r})$  is the final state wave function of the neutron- $\Lambda$  system and the variable  $S'$  is 0 or 1 for the singlet or triplet case.  $\mathbf{K}$  is the center-of-mass momentum of the baryon pair. The quantity  $|\Psi_D^{S_z}(\mathbf{r})\rangle$  is the deuteron wave function with an initial spin projection  $S_z$ . We obtain the radial deuteron wave function from the solution of the coupled Schrödinger equations for a pure one-pion-exchange potential. It has been shown that this interaction reproduces all of the low-energy properties of the deuteron [19, 20, 21] (likely to be the most important in this calculation). The operator  $\mathcal{O} = \boldsymbol{\sigma}_1 \cdot \boldsymbol{\epsilon}$ .

Transforming to relative and center-of-mass coordinates in the spatial variables we have

$$M^{S', S'_z, S_z} = (2\pi)^3 \delta(\mathbf{K} - \mathbf{k}) \int d\mathbf{r} \langle S' S'_z | \psi_{S'}^*(\mathbf{p}, \mathbf{r}) | \mathcal{O} e^{i\frac{\mathbf{k} \cdot \mathbf{r}}{2}} | \Psi_D^{S_z}(\mathbf{r}) \rangle. \quad (7)$$

We write the deuteron wave function as

$$|\Psi_D^{S_z}(\mathbf{r})\rangle = S(r)Y_0^0|1S_z\rangle + D(r)\sum Y_2^{m'}(\mathbf{r})|1\sigma\rangle C_{1,2,1}^{\sigma,m',S_z}, \quad (8)$$

and the  $\Lambda$ -n relative motion wave function as

$$\psi_{S'}(\mathbf{p}, \mathbf{r}) = 4\pi \sum i^\ell Y_\ell^m(\mathbf{r}) Y_\ell^{m*}(\mathbf{p}) \phi_\ell^{S'}(r). \quad (9)$$

With these expansions we can write (with an arbitrary overall normalization, omitting the delta function)

$$\begin{aligned} M^{S',S'_z,S_z} &= 4\pi \langle S'S'_z|\mathcal{O}|\int d\mathbf{r} \sum_{\ell,m,L,M} i^{L-\ell} Y_\ell^{m*}(\mathbf{r}) Y_L^M(\mathbf{r}) Y_\ell^m(\mathbf{p}) Y_L^{M*}(\mathbf{k}) \phi_\ell^{S'}(r) j_L\left(\frac{kr}{2}\right) \\ &\times [S(r)Y_0^0|1S_z\rangle + D(r)\sum Y_2^{m'}(\mathbf{r})|1\sigma\rangle C_{1,2,1}^{\sigma,m',S_z}] \end{aligned} \quad (10)$$

With the photon direction,  $\mathbf{k}$ , along the z axis, one has

$$Y_L^M(\mathbf{k}) = \delta_{M,0} \sqrt{\frac{2L+1}{4\pi}}. \quad (11)$$

Performing the integral over the angles of  $\mathbf{r}$ , we obtain

$$\begin{aligned} M^{S',S'_z,S_z} &= \sum_{\ell,m} Y_\ell^m(\mathbf{p}) [\langle S'S'_z|\mathcal{O}|1S_z\rangle \delta_{m0} \sqrt{2\ell+1} \int_0^\infty r^2 dr \phi_\ell^{S'}(r) j_\ell\left(\frac{1}{2}kr\right) S(r) \\ &+ \sum_{L,\sigma} i^{L-\ell} \sqrt{\frac{5(2L+1)}{(2\ell+1)}} C_{L,2,\ell}^{0,m,m} C_{L,2,\ell}^{0,0,0} \sqrt{2L+1} C_{1,2,1}^{\sigma,m,S_z} \langle S'S'_z|\mathcal{O}|1\sigma\rangle \\ &\times \int_0^\infty r^2 dr D(r) \phi_\ell^{S'}(r) j_L\left(\frac{kr}{2}\right)] \end{aligned} \quad (12)$$

or,

$$\begin{aligned} M^{S',S'_z,S_z} &= \sum_{\ell,m} Y_\ell^m(\mathbf{p}) [S_\ell(S') \delta_{m,0} \langle S'S'_z|\mathcal{O}|1S_z\rangle \\ &+ \sqrt{5} \sum_{\sigma} C_{1,2,1}^{\sigma,m,S_z} \langle S'S'_z|\mathcal{O}|1\sigma\rangle \sum_L i^{L-\ell} C_{\ell,2,L}^{m,-m,0} C_{\ell,2,L}^{0,0,0} D_{\ell,L}(S')] \end{aligned} \quad (13)$$

with the definitions

$$S_\ell(S') = \sqrt{2\ell+1} \int_0^\infty r^2 dr \phi_\ell^{S'}(r) j_\ell\left(\frac{kr}{2}\right) S(r) \quad (14)$$

$$D_{\ell,L}^{S'} = \sqrt{2\ell+1} \int_0^\infty r^2 dr D(r) \phi_\ell^{S'}(r) j_L\left(\frac{kr}{2}\right). \quad (15)$$

If we define

$$B_\ell^m(S') \equiv \sum_L i^{L-\ell} C_{\ell,2,L}^{m,-m,0} C_{\ell,2}^{0,0,0} D_{\ell,L}(S'), \quad (16)$$

we can write

$$M^{S',S'_z,S_z} = \sum_{\ell,m} Y_\ell^m(\mathbf{p}) \left[ S_\ell \delta_{m,0} \langle S' S'_z | \mathcal{O} | 1 S_z \rangle + \sqrt{5} \sum_\sigma C_{1,2,1}^{\sigma,m,S_z} \langle S' S'_z | \mathcal{O} | 1 \sigma \rangle B_\ell^m \right], \quad (17)$$

where the explicit dependence on  $S'$  of  $S_\ell$  and  $B_\ell^m$  has been suppressed.

We define the spherical components of the photon polarization vector as

$$\epsilon^{+1} = -\frac{1}{\sqrt{2}}(\epsilon_x + i\epsilon_y); \quad \epsilon^{-1} = \frac{1}{\sqrt{2}}(\epsilon_x - i\epsilon_y); \quad \epsilon^0 = \epsilon_z. \quad (18)$$

The spin structure of the radiative capture operator is assumed to be of the form

$$\mathcal{O} = \boldsymbol{\sigma}_1 \cdot \boldsymbol{\epsilon} \quad (19)$$

where particle 1 is the proton which is transformed into a  $\Lambda$ . The expectation values of this operator for the baryon spin states are

Triplet	
$\langle 1, 0   \mathcal{O}   1, 1 \rangle$	$\epsilon^+$
$\langle 1, 0   \mathcal{O}   1, -1 \rangle$	$-\epsilon^-$
$\langle 1, 0   \mathcal{O}   1, 0 \rangle$	0
$\langle 1, 1   \mathcal{O}   1, 1 \rangle$	$\epsilon^0$
$\langle 1, -1   \mathcal{O}   1, -1 \rangle$	$-\epsilon^0$
$\langle 1, 1   \mathcal{O}   1, 0 \rangle$	$-\epsilon^-$
$\langle 1, -1   \mathcal{O}   1, 0 \rangle$	$\epsilon^+$
$\langle 1, 1   \mathcal{O}   1, -1 \rangle$	0
$\langle 1, -1   \mathcal{O}   1, 1 \rangle$	0
Singlet	
$\langle 0, 0   \mathcal{O}   1, 1 \rangle$	$-\epsilon^+$
$\langle 0, 0   \mathcal{O}   1, -1 \rangle$	$-\epsilon^-$
$\langle 0, 0   \mathcal{O}   1, 0 \rangle$	$\epsilon^0$

The transversality condition gives  $\epsilon^0 = 0$ .

Because of the averaging over the direction of the unobserved momentum  $\mathbf{p}$ , each term in  $\ell$  and  $m$  will contribute incoherently. We now consider each of the cases  $m = 0$ ,  $m = \pm 1$  and  $m = \pm 2$  separately. In the square-averaging over the photon polarizations we omit the uniform factor of  $1/2$ .

### 2.2.1 $m=0$

For  $m = 0$

$$M_{m=0}^{S', S'_z, S_z} = \langle S' S'_z | \mathcal{O} | 1 S_z \rangle \sum_{\ell=0}^{\infty} Y_{\ell}^0(\mathbf{p}) (S_{\ell} + \sqrt{5} C_{1, 2, 1}^{S_z, 0, S_z} B_{\ell}^0) \quad (20)$$

This term will contribute to the transitions ( $S_z = \pm 1 \rightarrow S'_z = 0$ ) and ( $S_z = 0 \rightarrow S'_z = \pm 1$ )

$$M_{m=0}^{1, 0, -1} = -\epsilon^{-} \sum_{\ell=0}^{\infty} Y_{\ell}^0(\mathbf{p}) (S_{\ell} + \frac{1}{\sqrt{2}} B_{\ell}^0) = M_{m=0}^{0, 0, -1} \quad (21)$$

$$M_{m=0}^{1, 0, 1} = \epsilon^{+} \sum_{\ell=0}^{\infty} Y_{\ell}^0(\mathbf{p}) (S_{\ell} + \frac{1}{\sqrt{2}} B_{\ell}^0) = -M_{m=0}^{0, 0, 1} \quad (22)$$

$$M_{m=0}^{1, 1, 0} = -\epsilon^{-} \sum_{\ell=0}^{\infty} Y_{\ell}^0(\mathbf{p}) (S_{\ell} - \sqrt{2} B_{\ell}^0); \quad M_{m=0}^{1, -1, 0} = \epsilon^{+} \sum_{\ell=0}^{\infty} Y_{\ell}^0(\mathbf{p}) (S_{\ell} - \sqrt{2} B_{\ell}^0) \quad (23)$$

giving a contribution to the total capture rate of

$$\sum_{\ell=0}^{\infty} (S_{\ell} + \frac{1}{\sqrt{2}} B_{\ell}^0)^2 \quad (24)$$

from each of the initial magnetic states  $\pm 1$  for either the singlet or triplet final state and

$$2 \sum_{\ell=0}^{\infty} (S_{\ell} - \sqrt{2} B_{\ell}^0)^2 \quad (25)$$

from the initial magnetic state 0 for the triplet final state.

Since the singlet and triplet states add constructively for  $S_z = 1$  and destructively for  $S_z = -1$ , they are incoherent if and only if the populations of the these two initial states are equal.

### 2.2.2 $|m| = 1$

For  $|m| = 1$

$$M_{m=1}^{S', S'_z, S_z} = \langle S' S'_z | \mathcal{O} | 1 S_z - 1 \rangle \sqrt{5} C_{1, 2, 1}^{S_z - 1, 1, S_z} \sum_{\ell=1}^{\infty} Y_{\ell}^1(\mathbf{p}) B_{\ell}^1 \quad (26)$$

contributes to ( $S_z = 0 \rightarrow S'_z = 0$ );

$$M_{m=1}^{1, 0, 0} = -\epsilon^{-} \sqrt{\frac{3}{2}} \sum_{\ell=1}^{\infty} Y_{\ell}^1(\mathbf{p}) B_{\ell}^1 = M_{m=1}^{0, 0, 0} \quad (27)$$



and ( $S_z = 1 \rightarrow S'_z = \pm 1$ )

$$M_{m=1}^{1,1,1} = \epsilon^- \sqrt{\frac{3}{2}} \sum_{\ell=1}^{\infty} Y_{\ell}^1(\mathbf{p}) B_{\ell}^1; \quad M_{m=1}^{1,-1,1} = -\epsilon^+ \sqrt{\frac{3}{2}} \sum_{\ell=1}^{\infty} Y_{\ell}^1(\mathbf{p}) B_{\ell}^1 \quad (28)$$

while

$$M_{m=-1}^{S',S'_z,S_z} = \langle S' S'_z | \mathcal{O} | 1S_z + 1 \rangle \sqrt{5} C_{1,2,1}^{S_z+1,-1,S_z} \sum_{\ell=1}^{\infty} Y_{\ell}^{-1}(\mathbf{p}) B_{\ell}^1 \quad (29)$$

contributes to ( $S_z = 0 \rightarrow S'_z = 0$ );

$$M_{m=-1}^{1,0,0} = \epsilon^+ \sqrt{\frac{3}{2}} \sum_{\ell=1}^{\infty} Y_{\ell}^{-1}(\mathbf{p}) B_{\ell}^1 = -M_{m=-1}^{0,0,0} \quad (30)$$

and ( $S_z = -1 \rightarrow S'_z = \pm 1$ )

$$M_{m=-1}^{1,1,-1} = \epsilon^- \sqrt{\frac{3}{2}} \sum_{\ell=1}^{\infty} Y_{\ell}^{-1}(\mathbf{p}) B_{\ell}^1; \quad M_{m=-1}^{1,-1,-1} = -\epsilon^+ \sqrt{\frac{3}{2}} \sum_{\ell=1}^{\infty} Y_{\ell}^{-1}(\mathbf{p}) B_{\ell}^1 \quad (31)$$

giving a contribution from  $|m| = 1$  to the capture rate of

$$3 \sum_{\ell=1}^{\infty} \left( B_{\ell}^1 \right)^2; \quad \text{for each of } S_z = 0, \pm 1. \quad (32)$$

Only the  $S_z = 0$  state contributes for the singlet final state. Since the relative sign of the singlet and triplet is different for  $m = 1$  and  $m = -1$ , the singlet and triplet states are always incoherent for  $|m| = 1$ .

### 2.2.3 $|m| = 2$

For  $|m| = 2$

$$M_{m=2}^{S',S'_z,S_z} = \langle S' S'_z | \mathcal{O} | 1S_z - 2 \rangle \sqrt{5} C_{1,2,1}^{S_z-2,2,S_z} \sum_{\ell=2}^{\infty} Y_{\ell}^2(\mathbf{p}) B_{\ell}^2 \quad (33)$$

contributes to ( $S_z = 1 \rightarrow S'_z = 0$ )

$$M_{m=2}^{1,0,1} = -\epsilon^- \sqrt{3} \sum_{\ell=2}^{\infty} Y_{\ell}^2(\mathbf{p}) B_{\ell}^2 = M_{m=2}^{0,0,1} \quad (34)$$

while

$$M_{m=-2}^{S',S'_z,S_z} = \langle S' S'_z | \mathcal{O} | 1S_z + 2 \rangle \sqrt{5} C_{1,2,1}^{S_z+2,-2,S_z} \sum_{\ell=2}^{\infty} Y_{\ell}^{-2}(\mathbf{p}) B_{\ell}^2 \quad (35)$$

contributes to  $(S_z = -1 \rightarrow S'_z = 0)$ .

$$M_{m=-2}^{1,0,-1} = \epsilon^+ \sqrt{3} \sum_{\ell=2}^{\infty} Y_{\ell}^{-2}(\mathbf{p}) B_{\ell}^2 = -M_{m=-2}^{0,0,-1} \quad (36)$$

giving a contribution to the capture rate for either initial spin projection  $\pm 1$  of

$$3 \sum_{\ell=2}^{\infty} (B_{\ell}^2)^2 \quad (37)$$

Since the singlet and triplet states add constructively for  $S_z = 1$  and destructively for  $S_z = -1$ , they are incoherent only if the populations of the these two initial states are equal.

## 2.3 Summary

Combining the expressions in the previous section we obtain the following results for the capture rate for the various initial and final states. The notation for quantities calculated with the singlet or triplet final state on the  $\Lambda$ -n system is now shown explicitly. For the amplitudes in the form  $M_m^{S'_z, S_z}$

$$m = 0, \epsilon^-$$

$$M_0^{0,-1} = - \sum_{\ell=0}^{\infty} Y_{\ell}^0(\mathbf{p}) \left[ S_{\ell}(1) + \frac{1}{\sqrt{2}} B_{\ell}^0(1) + S_{\ell}(0) + \frac{1}{\sqrt{2}} B_{\ell}^0(0) \right] \quad (38)$$

$$M_0^{1,0} = - \sum_{\ell=0}^{\infty} Y_{\ell}^0(\mathbf{p}) \left( S_{\ell}(1) - \sqrt{2} B_{\ell}^0(1) \right) \quad (39)$$

$$m = 0, \epsilon^+$$

$$M_0^{0,1} = \sum_{\ell=0}^{\infty} Y_{\ell}^0(\mathbf{p}) \left[ S_{\ell}(1) + \frac{1}{\sqrt{2}} B_{\ell}^0(1) - S_{\ell}(0) - \frac{1}{\sqrt{2}} B_{\ell}^0(0) \right] \quad (40)$$

$$M_0^{-1,0} = \sum_{\ell=0}^{\infty} Y_{\ell}^0(\mathbf{p}) \left( S_{\ell}(1) - \sqrt{2} B_{\ell}^0(1) \right) \quad (41)$$

$$m = 1, \epsilon^-$$

$$M_1^{0,0} = -\sqrt{\frac{3}{2}} \sum Y_{\ell}^1(\mathbf{p}) \left[ B_{\ell}^1(1) + B_{\ell}^1(0) \right] \quad (42)$$

$$M_1^{1,1} = \sqrt{\frac{3}{2}} \sum Y_{\ell}^1(\mathbf{p}) B_{\ell}^1(1) \quad (43)$$

$$m = 1, \epsilon^+$$

$$M_1^{-1,1} = -\sqrt{\frac{3}{2}} \sum Y_\ell^1(\mathbf{p}) B_\ell^1(1) \quad (44)$$

$$m = -1, \epsilon^-$$

$$M_{-1}^{1,-1} = \sqrt{\frac{3}{2}} \sum_{\ell=0}^{\infty} Y_\ell^{-1}(\mathbf{p}) B_\ell^0(1) \quad (45)$$

$$m = -1, \epsilon^+$$

$$M_{-1}^{0,0} = \sqrt{\frac{3}{2}} \sum Y_\ell^{-1}(\mathbf{p}) [B_\ell^1(1) - B_\ell^1(0)] \quad (46)$$

$$M_{-1}^{-1,-1} = \sqrt{\frac{3}{2}} \sum Y_\ell^{-1}(\mathbf{p}) B_\ell^1(1) \quad (47)$$

$$m = 2, \epsilon^-$$

$$M_2^{0,1} = -\sqrt{3} \sum Y_\ell^2(\mathbf{p}) [B_\ell^1(1) + B_\ell^1(0)] \quad (48)$$

$$m = -2, \epsilon^+$$

$$M_{-2}^{0,-1} = \sqrt{3} \sum Y_\ell^{-2}(\mathbf{p}) [B_\ell^1(1) - B_\ell^1(0)] . \quad (49)$$

For the capture rates we have

$$\begin{aligned} S_z = 1; \quad & \sum_{\ell=0}^{\infty} \left[ S_\ell(1) + \frac{1}{\sqrt{2}} B_\ell^0(1) - S_\ell(0) - \frac{1}{\sqrt{2}} B_\ell^0(0) \right]^2 + 3 \sum_{\ell=1}^{\infty} [B_\ell^1(1)]^2 \\ & + 3 \sum_{\ell=2}^{\infty} [B_\ell^2(1) + B_\ell^2(0)]^2 \end{aligned} \quad (50)$$

$$S_z = 0; \quad 2 \sum_{\ell=0}^{\infty} [S_\ell(1) - \sqrt{2} B_\ell^0(1)]^2 + 3 \sum_{\ell=1}^{\infty} [B_\ell^1(1)]^2 + 3 \sum_{\ell=1}^{\infty} [B_\ell^1(0)]^2 \quad (51)$$

$$S_z = -1; \quad \sum_{\ell=0}^{\infty} \left[ S_\ell(1) + \frac{1}{\sqrt{2}} B_\ell^0(1) + S_\ell(0) + \frac{1}{\sqrt{2}} B_\ell^0(0) \right]^2 + 3 \sum_{\ell=1}^{\infty} [B_\ell^1(1)]^2$$

$$+ 3 \sum_{\ell=2}^{\infty} \left[ B_{\ell}^2(1) - B_{\ell}^2(0) \right]^2. \quad (52)$$

Using plane waves for  $\ell \geq 1$

$$S_z = 1; \quad \left\{ S_0(1) - S_0(0) + \frac{1}{\sqrt{2}} \left[ B_0^0(1) - B_0^0(0) \right] \right\}^2 + 3 \sum_{\ell=1}^{\infty} \left[ B_{\ell}^1 \right]^2 + 12 \sum_{\ell=2}^{\infty} \left[ B_{\ell}^2 \right]^2 \quad (53)$$

$$S_z = 0; \quad 2 \left[ S_0(1) - \sqrt{2} B_0^0(1) \right]^2 + 2 \sum_{\ell=1}^{\infty} \left[ S_{\ell}(1) - \sqrt{2} B_{\ell}^0(1) \right]^2 + 6 \sum_{\ell=1}^{\infty} \left[ B_{\ell}^1 \right]^2 \quad (54)$$

$$S_z = -1; \quad \left\{ S_0(1) + S_0(0) + \frac{1}{\sqrt{2}} \left[ B_0^0(1) + B_0^0(0) \right] \right\}^2 + 4 \sum_{\ell=1}^{\infty} \left[ S_{\ell} + \frac{1}{\sqrt{2}} B_{\ell}^0 \right]^2 + 3 \sum_{\ell=1}^{\infty} \left[ B_{\ell}^1 \right]^2 \quad (55)$$

Adding, and assuming all magnetic projections of the deuteron to be equally populated, we find

$$\begin{aligned} & 2 \left[ S_0(1) + \frac{1}{\sqrt{2}} B_0^0(1) \right]^2 + 2 \left[ S_0(0) + \frac{1}{\sqrt{2}} B_0^0(0) \right]^2 + 2 \left[ S_0(1) - \sqrt{2} B_0^0(1) \right]^2 \\ & + 6 \sum_{\ell=1}^{\infty} \left\{ \left[ S_{\ell} \right]^2 + \left[ B_{\ell}^0 \right]^2 \right\} + 12 \sum_{\ell=1}^{\infty} \left[ B_{\ell}^1 \right]^2 + 12 \sum_{\ell=2}^{\infty} \left[ B_{\ell}^2 \right]^2. \end{aligned} \quad (56)$$

Also useful are the expressions for a given photon polarization.

$\epsilon^-$

$$S_z = 1; \quad \frac{3}{2} \sum_{\ell=1}^{\infty} \left[ B_{\ell}^1 \right]^2 + 12 \sum_{\ell=2}^{\infty} \left[ B_{\ell}^2 \right]^2 \quad (57)$$

$$S_z = 0; \quad \left| S_0(1) - \sqrt{2} B_0^0(1) \right|^2 + \sum_{\ell=1}^{\infty} \left[ S_{\ell}(1) - \sqrt{2} B_{\ell}^0(1) \right]^2 + 6 \sum_{\ell=1}^{\infty} \left[ B_{\ell}^1 \right]^2 \quad (58)$$

$$S_z = -1; \quad \left| S_0(1) + S_0(0) + \frac{1}{\sqrt{2}} \left[ B_0^0(1) + B_0^0(0) \right] \right|^2 + 4 \sum_{\ell=1}^{\infty} \left[ S_{\ell} + \frac{1}{\sqrt{2}} B_{\ell}^0 \right]^2 + \frac{3}{2} \sum_{\ell=1}^{\infty} \left[ B_{\ell}^1 \right]^2 \quad (59)$$

$$\epsilon^+$$

$$S_z = 1; \quad \left| S_0(1) - S_0(0) + \frac{1}{\sqrt{2}} [B_0^0(1) - B_0^0(0)] \right|^2 + \frac{3}{2} \sum_{\ell=1}^{\infty} [B_\ell^1]^2 \quad (60)$$

$$S_z = 0; \quad \left| S_0(1) - \sqrt{2} B_0^0(1) \right|^2 + \sum_{\ell=1}^{\infty} [S_\ell(1) - \sqrt{2} B_\ell^0(1)]^2 \quad (61)$$

$$S_z = -1; \quad \frac{3}{2} \sum_{\ell=1}^{\infty} [B_\ell^1]^2. \quad (62)$$

## 2.4 Discussion

The ratio of the triplet to singlet rates, in the limit of s-wave contributions and an s-wave deuteron only, and assuming equal singlet and triplet scattering in the s-wave, is two. The introduction of the higher partial waves, and a difference in the scattering lengths, modifies this ratio but it is still roughly two. Hence there is a greater sensitivity to the triplet scattering length than to the singlet.

The S and D states of the deuteron interfere coherently, with different coefficients depending on whether the initial state is  $S_z = 0$  or  $S_z = \pm 1$ . For this reason the shape of the spectrum is different for the transition from the  $S_z = 0$  sub-state than from the  $S_z = \pm 1$  states due to the D-state contribution. Figure 1 shows a typical result for the pure  $\ell = 0$  contribution calculated with an asymptotic  $\Lambda$ -n wave function.

## 3 Solutions with Exponential Potentials

Rijken *et al.*[3] have recently fit potential models to the  $\Lambda$ -nucleon scattering data. We use the phase shifts for the s wave determined by this group to define our potentials so that the asymptotic form which is singular at the origin can be replaced with a more realistic wave function.

We will represent the effective interaction as a sum of exponential potentials. To this end we write the true potential as a Laplace transform

$$V(r) = \int_0^\infty \lambda(\mu) e^{-\mu r} d\mu. \quad (63)$$

Consider a calculation of this integral using a Gauss-Laguerre integration scheme with a 5 point approximation. The integral has maximum precision for only a single value of  $r$ , and the value that is chosen as typical for  $r$  represents the scale at which the integration is made. We choose to work, primarily, at the scale of 1 fm, in which case the points in the integration scheme (normally dimensionless) represent inverse ranges in units of  $\text{fm}^{-1}$ . The smallest of these inverse ranges has a value of  $0.26356 \text{ fm}^{-1}$ .

Since no exchange with such a small mass is believed to take place in this reaction, one expects to find zero for the coefficient of this term. Indeed, fits to the phase shifts produce very small numbers. We set these values to zero and consider fits with only 4 parameters. Thus, the potential is parameterized with the form

$$V(r) = \sum_{i=1}^4 \lambda_i e^{-\mu_i r}. \quad (64)$$

In this case the longest range entering into the problem is that of the second Gauss-Laguerre point, which has an inverse range of  $1.41340 \text{ fm}^{-1}$  and corresponds very well with two pion masses. The other ranges are  $3.59642 \text{ fm}^{-1}$ ,  $7.08581 \text{ fm}^{-1}$  and  $12.64080 \text{ fm}^{-1}$ . We have also considered the scale of one-half fm (which means that the inverse ranges are doubled in value) and 2 fm (which means that the inverse ranges have been multiplied by 1/2). While we work primarily with the fits on the scale of 1 fm, the alternate fits provide estimates of the model dependence. It is the 2 fm range fit which is more useful for reasons discussed in section 4.

### 3.1 Jost Solutions

Consider the solution of the Schrödinger equation for a sum of exponential potentials:

$$V(r) = \sum_{j=1}^N \lambda_j e^{-\mu_j r}. \quad (65)$$

Jost [22] writes the solution for the s-wave,  $f(p, r)$ , as

$$f(p, r) = e^{-ipr} \sum_{\gamma} C_{\gamma}(p) e^{-m_{\gamma} r} \quad (66)$$

where the subscript  $\gamma$  is a compound index representing a set of N integers. For example, for a three-term potential

$$\gamma \equiv [j, k, l], \quad j, k, l = 0, 1, 2, \dots \quad (67)$$

The coefficients  $C_{\gamma}(p)$  are given by the recursion relation

$$C_{[j,k,l]}(p) = \frac{\lambda_1 C_{[j-1,k,l]}(p) + \lambda_2 C_{[j,k-1,l]}(p) + \lambda_3 C_{[j,k,l-1]}(p)}{m_{\gamma}(m_{\gamma} + 2ip)}, \quad (68)$$

where

$$m_{\gamma} \equiv m_{[j,k,l]} \equiv j\mu_1 + k\mu_2 + l\mu_3. \quad (69)$$

The recursion is started with

$$C_{[0,0,0]} = 1, \quad C_{[-1,k,l]} = C_{[j,-1,l]} = C_{[j,k,-1]} = 0 \quad (70)$$

and is built up by first computing all coefficients with the sum of indices equal to one, then two, *etc.* with no negative index.

The solution with the proper boundary condition at the origin for an incoming spherical wave with unit amplitude at infinity is

$$\psi(p, r) = -\frac{f(p, r) - S(p)f(-p, r)}{2ipr}, \quad (71)$$

where

$$S(p) = \frac{f(p, 0)}{f(-p, 0)}. \quad (72)$$

These expressions can be used to calculate the values of the S-matrix for any value of  $p$ .

In order to calculate the overlap with the deuteron wave function, we require the wave function for real (positive) values of  $p$ . In this case we can write (for real  $\lambda_j$ )

$$f(-p, r) = f^*(p, r) \quad \text{with} \quad S(p) = e^{2i\delta(p)}. \quad (73)$$

We can now write the wave function (Eq. 71) as

$$\psi(p, r) = -\frac{e^{i\delta(p)}}{2ipr} \left[ e^{-i\delta(p)} e^{-ikr} \sum_{\gamma} C_{\gamma}(p) e^{-m_{\gamma}r} - e^{i\delta(p)} e^{ikr} \sum_{\gamma} C_{\gamma}(-p) e^{-m_{\gamma}r} \right]. \quad (74)$$

Note that the lowest order term is given by

$$\frac{e^{i\delta(p)} \sin(pr + \delta(p))}{pr}, \quad (75)$$

which is identical to the asymptotic wave function. We shall use these results to represent the  $\Lambda$ -n wave functions.

## 3.2 Fits to the Phase Shifts

Potentials were fit to the phase shifts[23] for each of the six cases of Ref. [3], for both the singlet and triplet states and for each of the scales mentioned above. Even though the interaction of interest is for  $\Lambda$ -neutron scattering, the fits were made to the  $\Lambda$ -proton phase shifts since they were more closely related to data. The results are shown in Fig. 2 for the triplet case. The potentials themselves are shown in Fig. 3. Table 1 lists the strengths from the fit for the scale of 1 fm. It is this fit which is used in the remainder of the paper unless otherwise noted.

<b>Singlet</b>				
Case	$\lambda_1$	$\lambda_2$	$\lambda_3$	$\lambda_4$
a	-0.26431	-45.03399	304.25626	2327.48169
b	-0.25513	-52.52803	352.90689	3036.24731
c	-0.30427	-59.00891	396.75662	3540.90601
d	-0.26357	-72.61646	499.84998	5000.94873
e	-0.26643	-79.84088	561.22314	5784.05615
f	-0.27467	-87.65697	643.43768	6791.61670
<b>Triplet</b>				
a	-0.43381	-35.94874	-0.17723	2502.01367
b	-0.42795	-37.85583	9.45284	2803.92017
c	-0.43581	-39.68054	32.58380	2944.07300
d	-0.44061	-41.15301	52.91377	3138.80127
e	-0.40514	-43.49734	77.60744	3344.70093
f	-0.35775	-46.00097	104.79501	3541.92969

Table 1: Values of the parameters used in the fit for the scale of 1 fm.

<b>Singlet</b>					
Case	$a$ (Rijken <i>et al.</i> )	$a$ (1 fm)	$r_0$ (1 fm)	$a$ (2 fm)	$r_0$ (2 fm)
a	-0.71	-0.73	6.71	-0.63	4.58
b	-0.90	-0.92	5.57	-0.82	3.99
c	-1.20	-1.23	4.55	-1.11	3.52
d	-1.71	-1.74	3.71	-1.59	2.99
e	-2.10	-2.16	3.46	-1.97	2.57
f	-2.51	-2.59	3.29	-2.36	2.68
<b>Triplet</b>					
a	-2.18	-2.21	2.99	-2.07	2.57
b	-2.13	-2.16	3.05	-2.03	2.71
c	-2.08	-2.10	3.15	-1.97	2.68
d	-1.95	-1.97	3.33	-1.84	2.84
e	-1.86	-1.86	3.40	-1.74	2.94
f	-1.75	-1.74	3.42	-1.65	3.03

Table 2: Values of the scattering length ( $a$ ) and effective range ( $r_0$ ) from the fits described.



Table 2 summarizes the scattering lengths and effective ranges corresponding to these fits. Also given are the scattering lengths found by Rijken *et al.* with the original potential.

In Fig. 4 are plotted the full wave function and the asymptotic wave function for the singlet “a” case of Ref. [3].

## 4 Results

We now turn to problems in the analysis and some possible solutions. The first issue is the use of the effective range expansion (ERE). In the  $\pi^- d \rightarrow nn\gamma$  measurement the ERE is adequate to describe the s-wave phase shift over the full range of data being analyzed. As is shown in Figure 5, this may not be the case for the  $n\Lambda$  measurement. Certainly it is not adequate over the full range, and it may be somewhat questionable even if only the upper 10 MeV of the spectrum is used. Of course the ERE is only useful if the asymptotic wave functions are used or if the short-range corrections are made with a technique similar to that employed in Ref. [9].

To find an alternative to the ERE we examined the parameters which came from the fitting of the exponential potentials to the phase shifts of Rijken *et al.* It was found that an acceptable fit could be obtained with the longest range parameter held fixed. Plots of the other three parameters (see Fig. 6 for the triplet case) show a linear behavior with case number. We therefore defined continuous variables, which reproduce the phase shifts (to a good approximation) at the integers 1 through 6 (corresponding to cases a through f), and create an interpolation and extrapolation procedure.

We define strengths

$$\lambda_i = c_i + x d_i \quad (76)$$

for  $i=2, 3, 4$ . Here  $x = x_s$  for the singlet case and  $x = x_t$  for the triplet case. The values of  $c_i$ ,  $d_i$  and  $\lambda_1$  are given in Table 3. While this method allows a range of scattering lengths to be produced with an appropriate short-range wave function, there are limitations. Since we would like to be able to study scattering lengths outside the range given in Ref. [3], we wish to consider values of  $x$  outside the range (1-6). Indeed this does give an extension of the range of scattering lengths, but for the 1 fm scale the range is limited. Outside this range the scattering lengths return to previous values. This constraint dictates the limits of the analysis shown in the figures to follow. It was found for the fits on the scale of 1/2 fm that the problem was greater, so that the analysis would be restricted to an even smaller area. The 2 fm range fits were used for the model dependence estimates because, in this case, a larger range of scattering lengths was feasible. However, the scattering lengths do not reproduce those of Ref. [3] as well as the 1 fm scale, as may be seen in Table 2.

In performing the analysis one may use the asymptotic wave functions or the full wave functions. The use of the full wave functions should be preferable, but one can obtain an idea of the sensitivity to the details of the full wave function by comparing

	$\lambda_1$	$c_2$	$d_2$	$c_3$	$d_3$	$c_4$	$d_4$
Singlet	-0.26431	-36.410	-8.624	235.36	68.90	1457.6	869.9
Triplet	-0.43381	-34.576	-1.373	-16.90	16.73	2321.4	180.6

Table 3: Values of the parameters for the linear representation of the potentials.

<b>Singlet</b>				
Case	$\lambda_1$	$\lambda_2$	$\lambda_3$	$\lambda_4$
1	-0.26431	-45.03399	304.25626	2327.48169
2	-0.26431	-52.14749	349.97018	3001.88623
3	-0.26431	-61.00436	417.78851	3645.56372
4	-0.26431	-72.61623	499.85406	5005.63232
5	-0.26431	-79.96191	562.18121	5807.02148
6	-0.26431	-88.15266	648.76056	6839.37939
<b>Triplet</b>				
1	-0.43381	-35.94874	-0.17723	2502.01367
2	-0.43381	-37.67183	9.01196	2795.74268
3	-0.43381	-39.68257	32.59604	2939.50488
4	-0.43381	-41.09288	52.92378	3138.51001
5	-0.43381	-42.13403	69.27229	3286.15967
6	-0.43381	-42.81454	83.45535	3404.96362

Table 4: Values of the parameters obtained for the 1 fm fit with constant  $\lambda_1$ .

results with those for the asymptotic wave functions. Figure 7 shows the sum of the  $S_z = 0$  and  $S_z = \pm 1$  s-wave contributions to the spectra as shown in Fig. 1 for the asymptotic wave functions (solid lines) and the full wave functions (dashed lines) for the parameters of the singlet “a” and “f” cases.

Perhaps the largest problem in the measurement is the separation of the singlet and triplet scattering lengths in the final state. If no spin degrees of freedom are measured then the singlet and triplet states contribute incoherently to the rate, and it might seem impossible to separate them. However, because the interference between the S and D states of the deuteron differs, the shapes of the singlet and triplet spectra are different, as illustrated in Fig. 8. Because the triplet gives a larger contribution than the singlet, a greater sensitivity to the triplet scattering is seen in the fits of the data and pseudo-data in the figures which follow.

Figure 9 shows an analysis of the data of Gall *et al.*[16]. Since this experiment was only a feasibility study, one can not expect to obtain much information about the scattering lengths. It is interesting to see, however, that the values are in the range expected. The open circle in the upper left hand corner shows the point of minimum  $\chi^2$ .

Figure 10 shows a similar analysis of the Gall *et al.* data with the 2 fm scale fits. In

this case a larger range of scattering lengths can be studied so that an error estimate can be given. One-standard-deviations limits can be read from the graph (the inner contour) with the triplet length lying between  $-1.3$  and  $-2.6$  fm and the singlet length between  $-0.2$  and  $-6.3$  fm.

Figure 11 provides a comparison of the experimental and theoretical spectra for the scattering lengths corresponding to the minimum  $\chi^2$  ( $=37.8$  for 37 data points) at  $a_s = -2.96$  and  $a_t = -1.72$  for the 1 fm scale.

Figure 12 presents a similar analysis of a pseudo data spectrum. The pseudo data were generated from a selected spectrum by including errors chosen from a Gaussian distribution such that they have a value of 3% of the rate at the maximum and are proportional to the square root of the rate at other points, as would be the case with errors dominated by counting statistics. The analyses shown were made over the full range of the Gall *et al.* data from 255 to 293 MeV unless otherwise specified. The case chosen for presentation in Fig. 12 is a favorable one in the sense that the scattering lengths used for generation of the pseudo-data (solid circle) fall near the center of the inner ellipse. As is necessary statistically, most of the results do fall nearer the edge of this ellipse with about 1/3 falling outside. One can observe from this figure that the experimental uncertainty in such an experiment would be  $\sim \pm 0.3$  fm for the triplet scattering length and  $\sim \pm 0.8$  fm for the singlet.

It is possible to use such an analysis of pseudo data to estimate errors due to model assumptions. For the following we use the same pseudo data that were described above. Figure 13a shows the results of an analysis using asymptotic wave functions with phase shifts determined from the Jost solutions. Figure 13b shows an analysis with the additional approximation that the phase shifts are taken from the ERE. As can be seen a significant error results.

Use of the asymptotic wave functions is an extreme approximation. Although we do not know exactly which more realistic wave function should be used, we can choose one among the Jost models we have been considering. To this end we analyze the spectrum created with the 1 fm scale using the 2 fm scale spectra. The result can be seen in Fig. 14. The positions of the singlet and triplet scattering lengths at the minimum are  $-1.613$  and  $-1.884$  fm to be compared with the values found with the (1 fm scale) analysis above of  $-1.896$  and  $-2.031$  fm (the input values are  $-1.968$  and  $-1.827$  fm). Thus we find model errors of  $\pm 0.28$  fm for the singlet and  $\pm 0.15$  fm for the triplet case. We will take these as estimates of the model (theoretical) errors.

Figure 15 shows the same type of analysis but including only the upper 10 MeV of the spectrum in the comparison. It is seen that the results are very similar, due perhaps to the fact that the main difference in shapes between singlet and triplet occurs in this region (see Fig. 8). The analysis over this range may offer experimental advantages in addition, since the background due to neutral pion decay is less severe.

We have seen that it is difficult to determine the scattering lengths individually. It is possible to separate the singlet and triplet states with the use of spin information

from the deuteron initial state or the photon final state. Figure 16 shows the spectra for the six possible combinations of these spin projections for four selected parameter sets. While the overall normalization of these curves is arbitrary, the relative normalization among them is correct. The upper left hand curve (for  $S_z = +1$  and right circularly polarized photon) shows the maximum sensitivity since it corresponds to the case where the singlet and triplet final states are coherent in a destructive manner. The disadvantage is that this same cancellation leads to a small rate if the singlet and triplet scatterings are not too dissimilar, as can be expected from SU(6) symmetry. However, this small quantity is a direct measure of the *difference between the singlet and triplet lengths*. Note that the spectra from an initial state  $S_z = 0$  are independent of the singlet parameters.

We can express the results in terms of more conventional variables. Figure 17 illustrates the spectrum expected from a pure vector polarized deuteron target with the asymmetry defined as

$$A_y \equiv \frac{\Gamma(S_z = +1) - \Gamma(S_z = -1)}{\Gamma(S_z = +1) + \Gamma(S_z = -1)}. \quad (77)$$

We see that a measurement with precision of the order of 2% is needed near the peak of the spectrum or 10% at the upper part of the spectrum. What is being searched for is a deviation of the asymmetry from  $-1$  or, in other words, a non-null value of the rate from the initial state  $S_z = +1$ . Such an observation would prove that the two scattering lengths are unequal. The dashed curve corresponds to a difference of 0.1 fm, the dash-dot curve to 0.66 fm, the solid curve to 0.91 fm and the dotted curve to 1.46 fm. This result is almost completely free from the model dependent effects discussed previously. The observation of a difference from  $-1$  in the asymmetry would be a direct indication of a difference in the scattering lengths.

Figure 18 shows the spectra expected from measurements in which the circular polarization of the final photon is measured. The asymmetry is defined as

$$A_\epsilon \equiv \frac{\Gamma(\epsilon = +1) - \Gamma(\epsilon = -1)}{\Gamma(\epsilon = +1) + \Gamma(\epsilon = -1)}. \quad (78)$$

Here again the same order of accuracy is needed to separate the dotted and dashed curves.

## 5 Conclusions

A formalism has been presented with attention to the spin degrees of freedom. Due to the difference in shape of the spectrum for the reaction proceeding from the zero magnetic quantum number projection of the deuteron from that with magnetic quantum numbers of  $\pm 1$ , the singlet-triplet separation can be made, although the difference is not large and the triplet state tends to dominate.

An analysis of the present data which exist for this reaction[16] has been made. Even though the uncertainties in the data from this feasibility experiment are large, some information can be obtained; in particular, separate numbers can be extracted for the singlet and triplet scattering lengths (with large overlapping errors). We find for the singlet scattering length in the range  $-0.15$  to  $-5.0$  and the triplet value from  $-1.3$  to  $-2.65$  (from the 2 fm range fit).

While this precision may seem rather modest, it is useful to compare with current values in the literature. Tan[24] obtained a value (believed to be mostly the triplet scattering length) of  $-2.0 \pm 0.5$  fm from an analysis of data on the reaction  $K^-d \rightarrow \pi^-p\Lambda$ . Recent data[17] on the reaction  $pp \rightarrow pK^+\Lambda$ , in conjunction with previous elastic scattering data[2], lead to a value for the spin-averaged scattering length of  $-2.0 \pm 0.2$  fm[17]. The importance of the influence of the third strongly interacting particle in the final state is difficult to estimate and the errors are experimental only.

In a three-body calculation for the hyper-triton bound state Miyagawa concludes[25] that the best values of the singlet scattering length lie between  $-2.7$  fm and  $-2.4$  fm and the triplet between  $-1.6$  fm and  $-1.3$  fm, conforming to the “f” solution of Rijken *et al.*[3].

An analysis of pseudo data for a  $K^-d \rightarrow \Lambda n\gamma$  experiment with a cross-comparison of models leads to an estimate of the model dependence of the order of  $\pm 0.2$  fm. The same type of study gives an estimate of the error in such an experiment of  $\pm 0.3$  fm for the triplet scattering length and  $\pm 0.8$  fm for the singlet. These estimates are for measurements without spin information and assume an uncertainty of 3% for the maximum rate in the spectrum.

It was shown that spin information in either the initial or final state would be valuable in separating the scattering lengths. If it were possible to perform the capture experiment on a deuteron target of purely magnetic quantum number zero the triplet scattering length alone would be measured.

The use of a polarized deuteron target would also allow the separation since the singlet and triplet states interfere destructively or constructively according to the relative alignment of the deuteron spin along or against the direction of the photon.

Since the previous feasibility study showed that the measurement was possible but very difficult, one might ask if the increased difficulty due to the requirement of polarizing the deuteron might not make it impossible. Certainly it adds another constraint, especially if it is necessary to add high-Z material which would preferentially capture the Kaons. In this regard we mention a possible polarized deuteron target which is made from a hydrogen-deuteron molecular system[26, 27]. It has a high density and contains no heavy materials.

For a measurement of the circular polarization of the photon, the spectra show a significant sensitivity of a similar type.

This work was supported by the U. S. Department of Energy and the National Science Foundation. HKH thanks the Korean Scientific and Engineering Foundation

for their support. The research of BFG was supported by the Department of Energy (LA-UR-99-6261).

## References

- [1] S. A. Coon, H. K. Han, J. Carlson, B. F. Gibson, Proceedings of “Mesons and Light Nuclei 98”, p. 407, World Scientific, Singapore
- [2] See Ref. [3] for a set of references to the data.
- [3] Th. A. Rijken, V. G. J. Stoks and Y. Yamamoto, *Phys. Rev. C* **59**, 21(1999)
- [4] A. Reuber, K. Holinde and J. Speth, *Nucl. Phys.* **A57**, 543(1994)
- [5] R. H. Phillips and K. M. Crowe, *Phys. Rev.* **96**, 484(1954)
- [6] K. McVoy, *Phys. Rev.* **121**, 1401(1961)
- [7] M. Bander, *Phys. Rev.* **134**, B1052(1964)
- [8] R. W. Salter, R. P. Hadock, Z. Zeller, D. R. Nygren and J. B. Czirr, *Nucl. Phys.* **A254**, 241(1975)
- [9] W. R. Gibbs, B. F. Gibson and G. Stephenson, *Phys. Rev. C* **11**, 90(1975)
- [10] O. Schori, B. Gabioud, C. Joseph, J. P. Perroud, D. Rüegger, M. T. Tran, P. Truöl, E. Winkelmann and W. Dahme, *Phys. Rev. C* **35**, 2252(1987); B. Gabioud *et al.*, *Nucl. Phys.* **A420**, 9(1981)
- [11] W. Tornow *et al.*, *Nucl. Phys.* **A631**, 421c(1998); C. R. Howell *et al.*, *Phys. Lett. B* **444**, 252(1998)
- [12] B. F. Gibson, G. J. Stephenson, V. R. Brown, and M. S. Weiss, BNL Report 18335, 1973
- [13] R. L. Workman and H. W. Fearing, *Phys. Rev. C* **41**, 1688(1990)
- [14] A. I. Akhiezer, G. I. Gakh, A. P. Rekalov and M. P. Rekalov, *Yad. Fiz.* **27**, 214(1978) [*Sov. J. Nucl. Phys.* **27**, 115(1978)]
- [15] R. Williams, C.-R. Ji and S. R. Cotanch, *Phys. Rev. C* **41**, 1449(1990); *Phys. Rev. C* **43**, 452(1991)
- [16] K. P. Gall *et al.*, *Phys. Rev. C* **42**, R475(1990)
- [17] J. T. Balewski *et al.*, *Eur. Phys. J. A* **2**, 99(1998); *Phys. Lett. B* **420**, 211(1998)
- [18] W. S. C. Williams, “An Introduction to Elementary Particles”, First Edition, Academic Press, New York and London, 1961, p. 374
- [19] T. E. O. Ericson and M. Rosa-Clot, *Nucl. Phys.* **A405**, 497(1983)
- [20] J. L. Friar, B. F. Gibson and G. L. Payne, *Phys. Rev. C* **30**, 1084(1984)

- [21] J. L. Ballot and M. R. Robilotta, *Phys. Rev.* **C45**, 986(1992); *Phys. Rev.* **C45**, 990(1992); J. L. Ballot, A. M. Eiró and M. R. Robilotta, *Phys. Rev.* **C40**, 1459(1989)
- [22] R. Jost, *Helv. Phys. Acta.* **20**, 256(1947)
- [23] V. Stoks, Private Communication
- [24] Hai Ho Tan, *Phys. Rev. Lett.* **23**, 395(1969)
- [25] K. Miyagawa, Proceedings of the First Asian Few Body Conference
- [26] A. Honig, Q. Fan, X. Wei, A. M. Sandorfi and C. S. Whisnant, “7th Workshop on Polarized Target Materials and Techniques”, Bad Honnef, Germany, June 20-22, 1994. Nucl. Instrum. and Meth. A356, 39(1995)
- [27] A. Honig, Q. Fan, X. Wei, Breuer, J. P. Didelez, M. Rigney, M. Lowry, A. M. Sandorfi, A. Lewis and C. S. Whisnant, “Twelfth Intl. Symp. on High Energy Spin Physics”, Amsterdam, Sept. 1996, ”Spin96” Conf. Proceedings, World Scientific 1997, p. 365

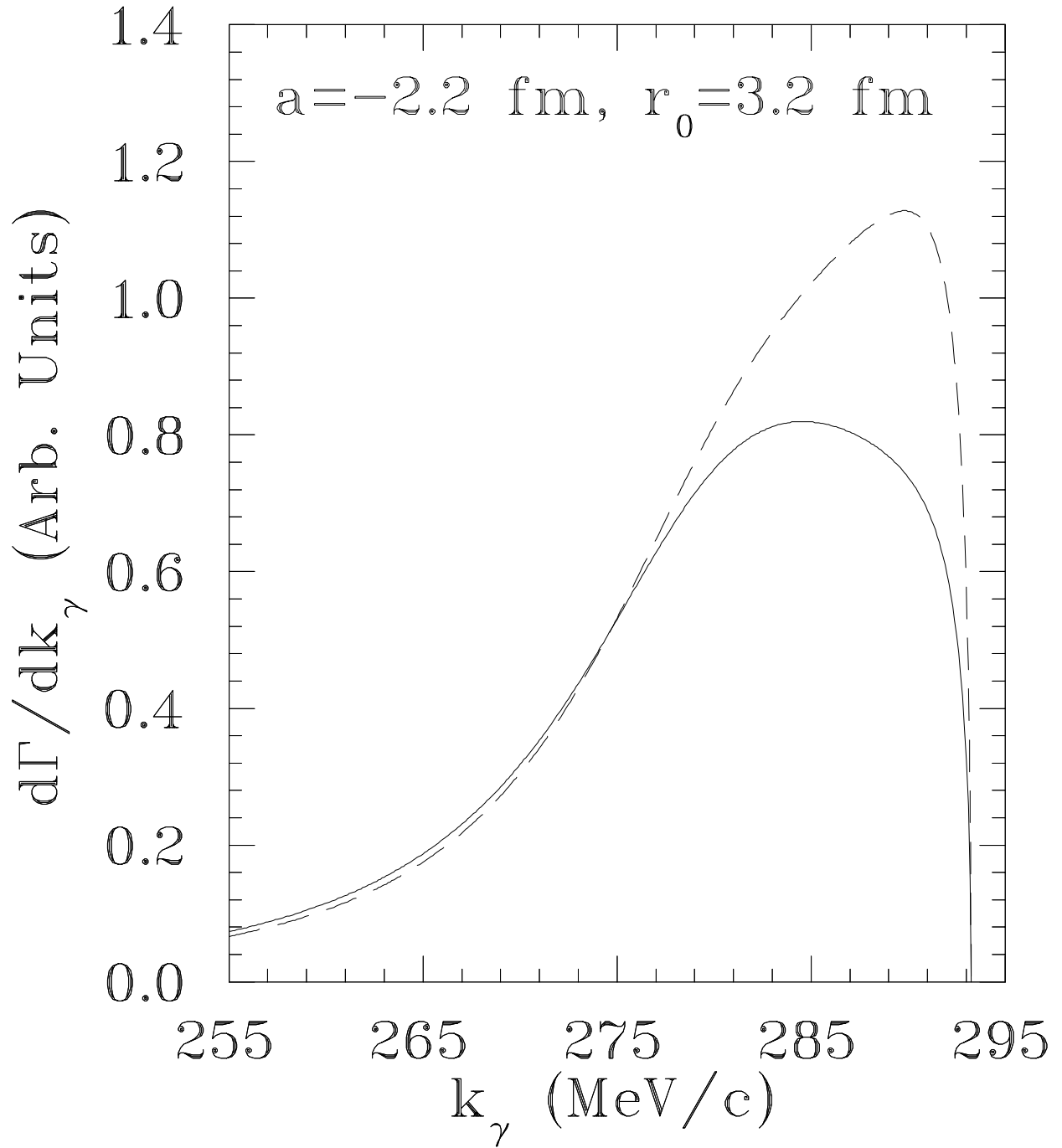


Figure 1: Comparison of the spectrum from the  $S_z = 0$  state with that from the non-zero initial projections. The dashed curve is the spectrum from the  $S_z = 0$  magnetic sub-state of the deuteron.



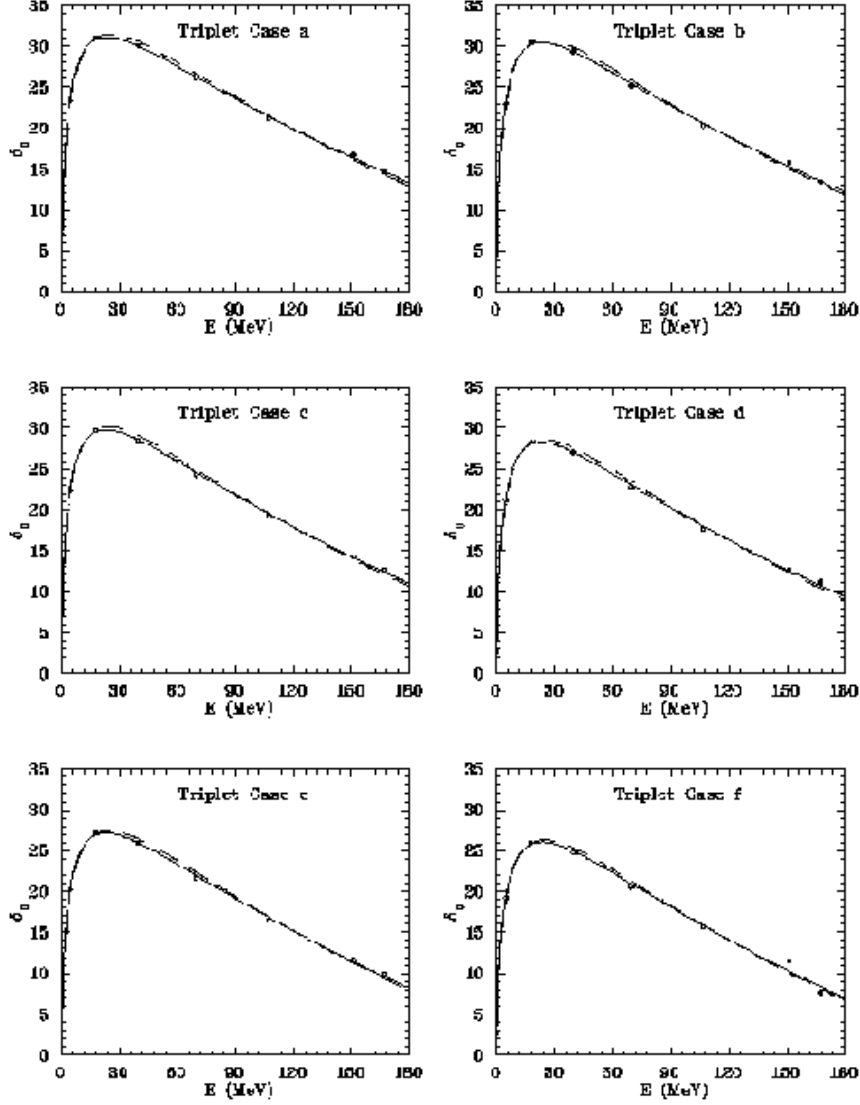


Figure 2: Comparison of the fits for the s-wave phase shifts with the results of Ref. [3] for the triplet states. The results for the scale of 1 fm is represented by the solid line and the scale of 2 fm by the dashed line.

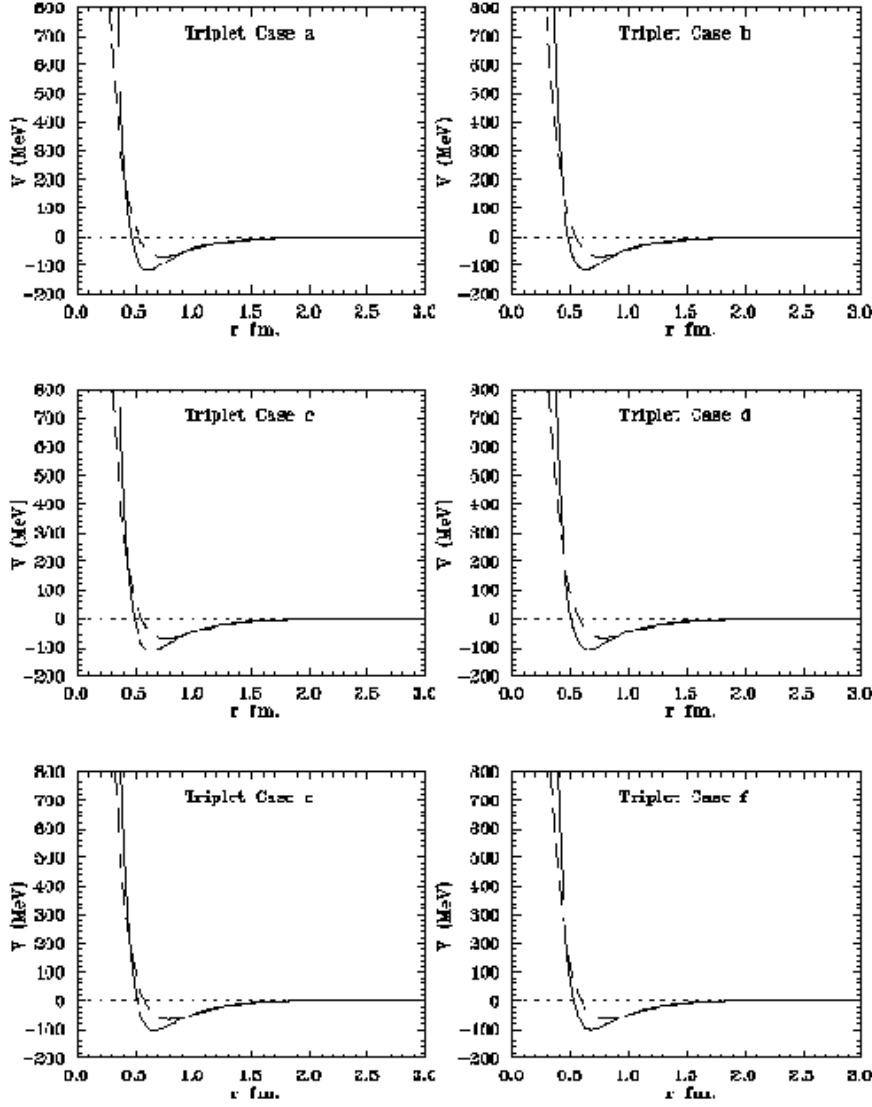


Figure 3: Potentials obtained from the fits for the triplet case. The meaning of the solid and dashed lines is the same as in Fig. 2.

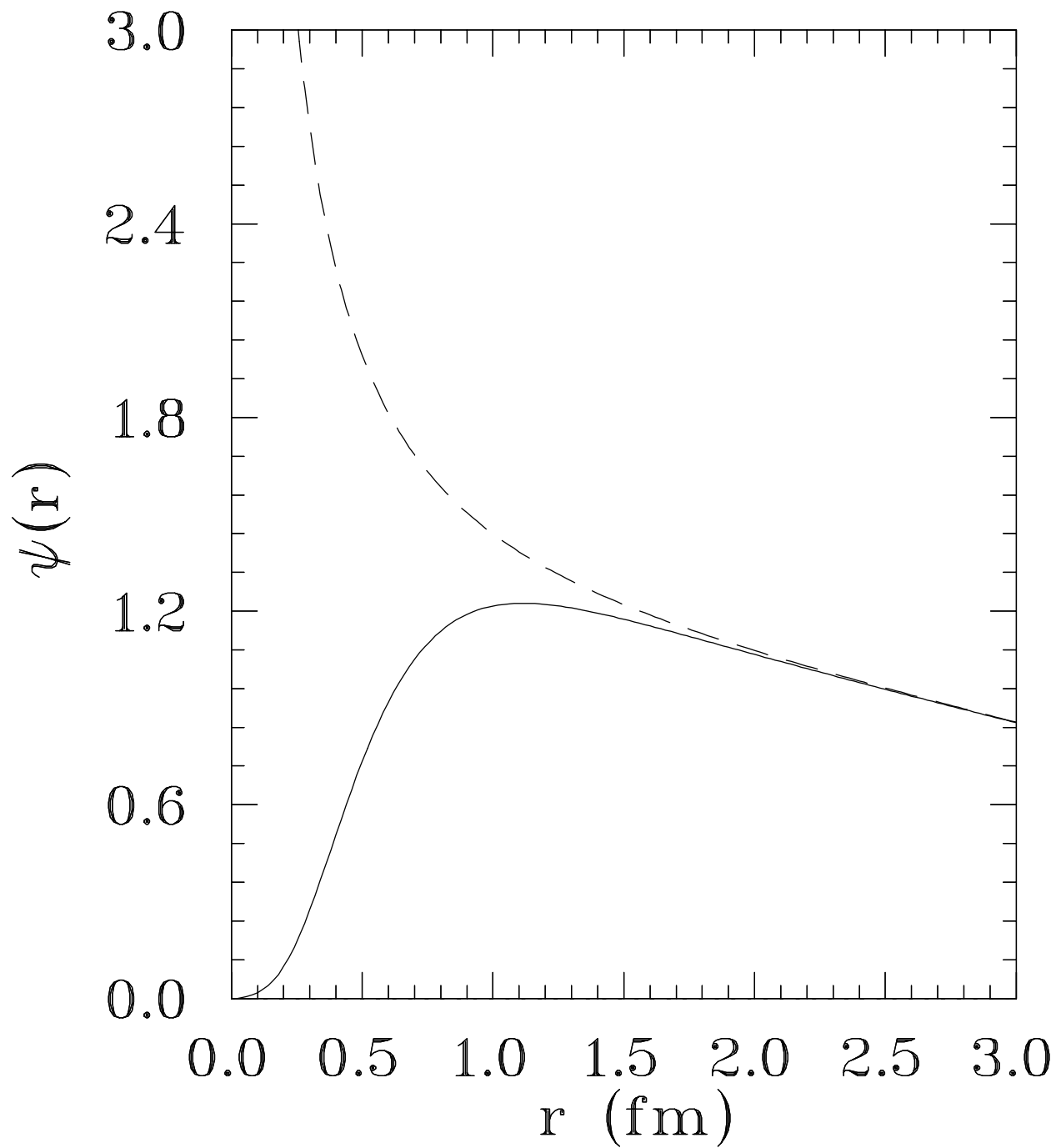


Figure 4: Wave function for the asymptotic wave function (dashed curve) compared with the Jost solution (solid curve).

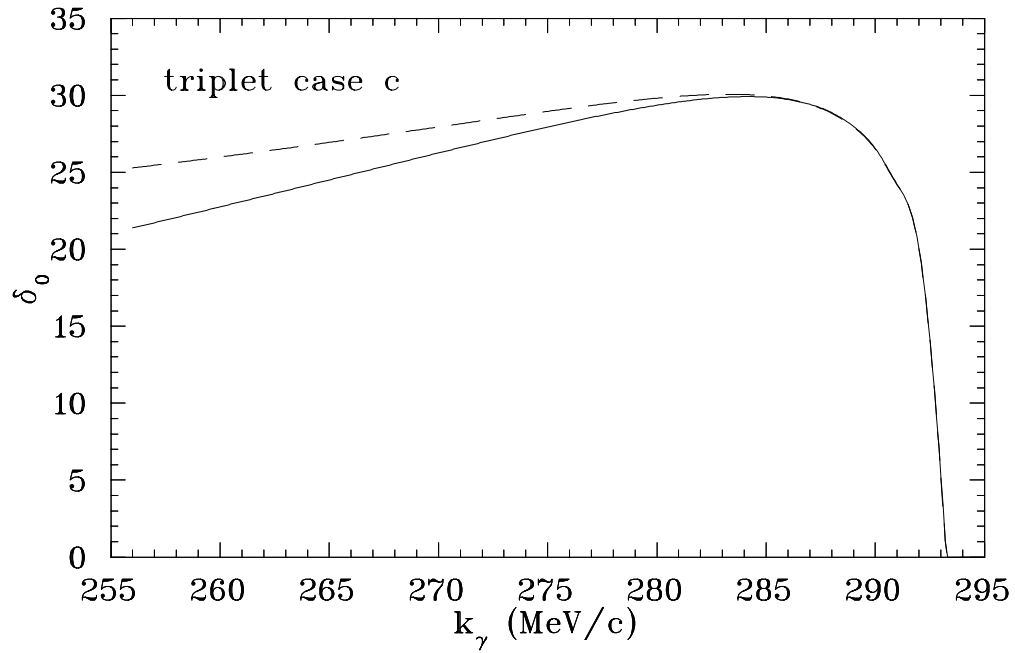
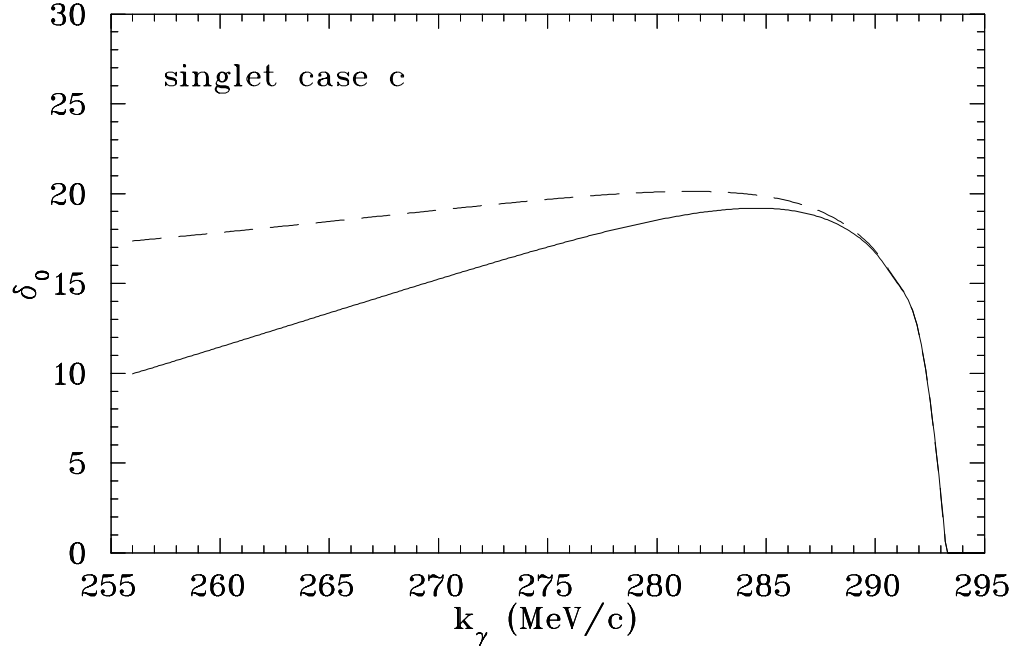


Figure 5: Phase shifts from the fitted potentials (solid) and from the effective range expansion (dashed) for the case c of Rijken *et al.* for the singlet and triplet cases.

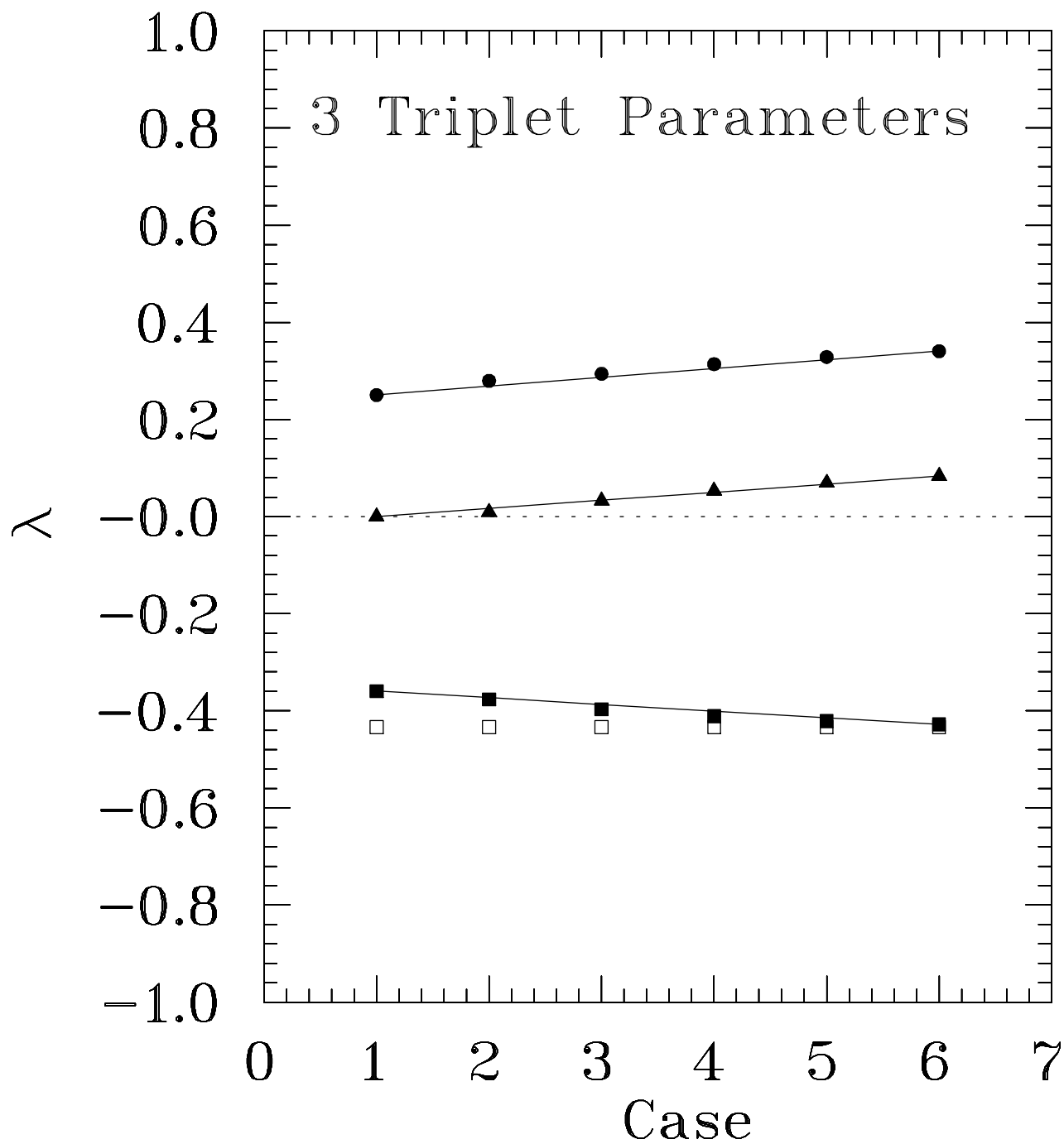


Figure 6: Parameters from the fit to the phases shifts of Rijken et al. showing the linear representation for the triplet case.

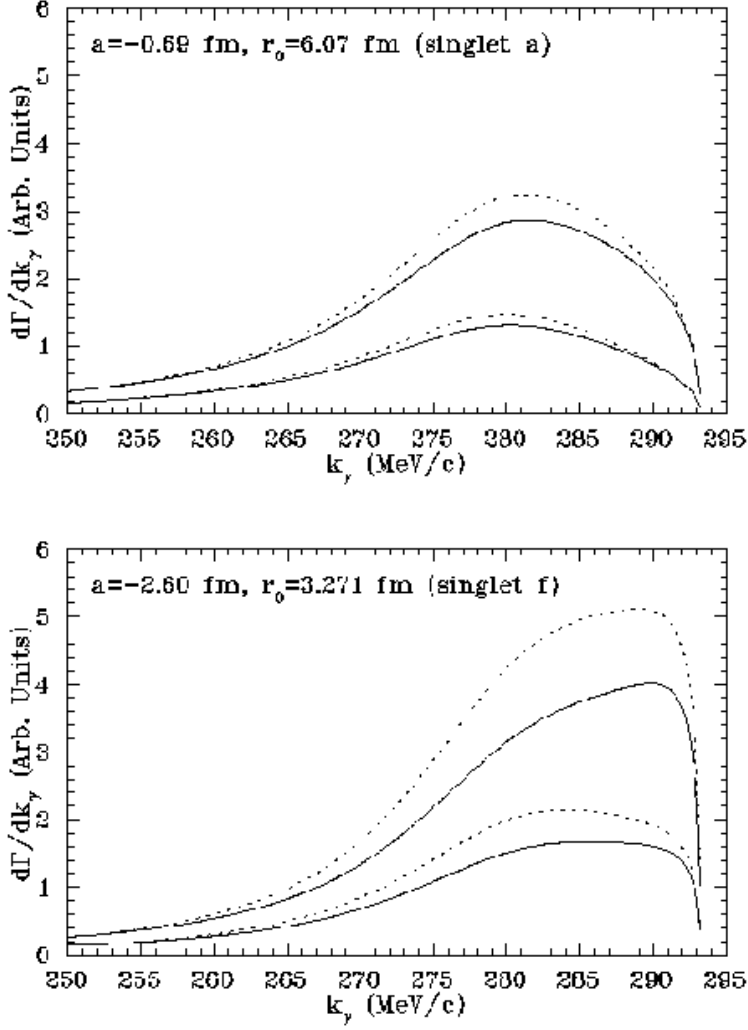


Figure 7: Comparison of the spectra expected ( $\ell = 0$  contribution only) with an asymptotic wave function (solid curves) with that using a solution to the Schrödinger equation (dotted curves) for the Jost parameters corresponding to cases “a” and “f” for the singlet final state. The lower curves are those resulting for the singlet spectrum and the upper ones are for the triplet spectrum.

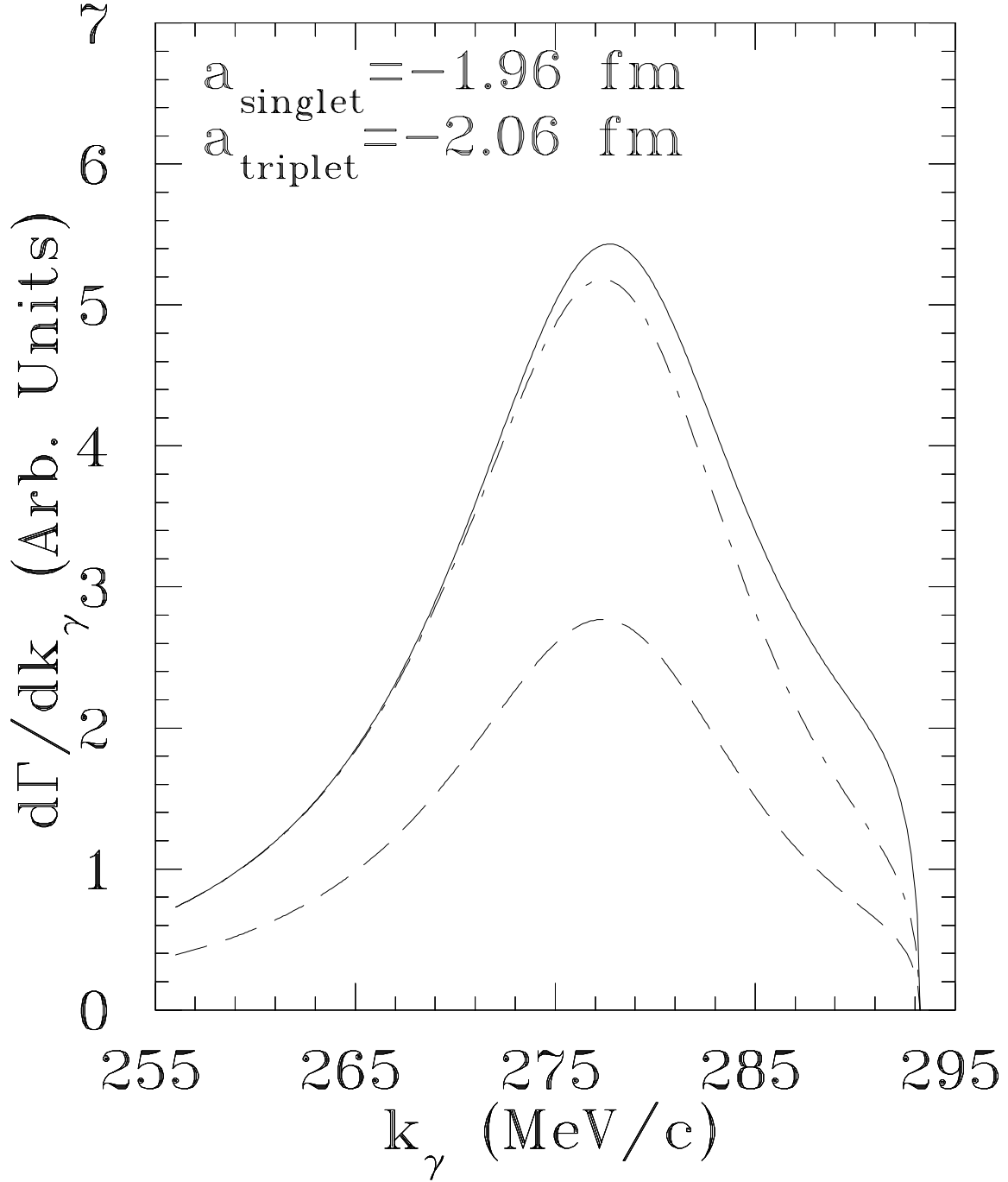


Figure 8: Comparison of singlet (dashed) and triplet (solid) spectra for a full calculation with realistic wave functions. The dash-dot curve shows the singlet spectrum renormalized to the triplet at the lowest energy.

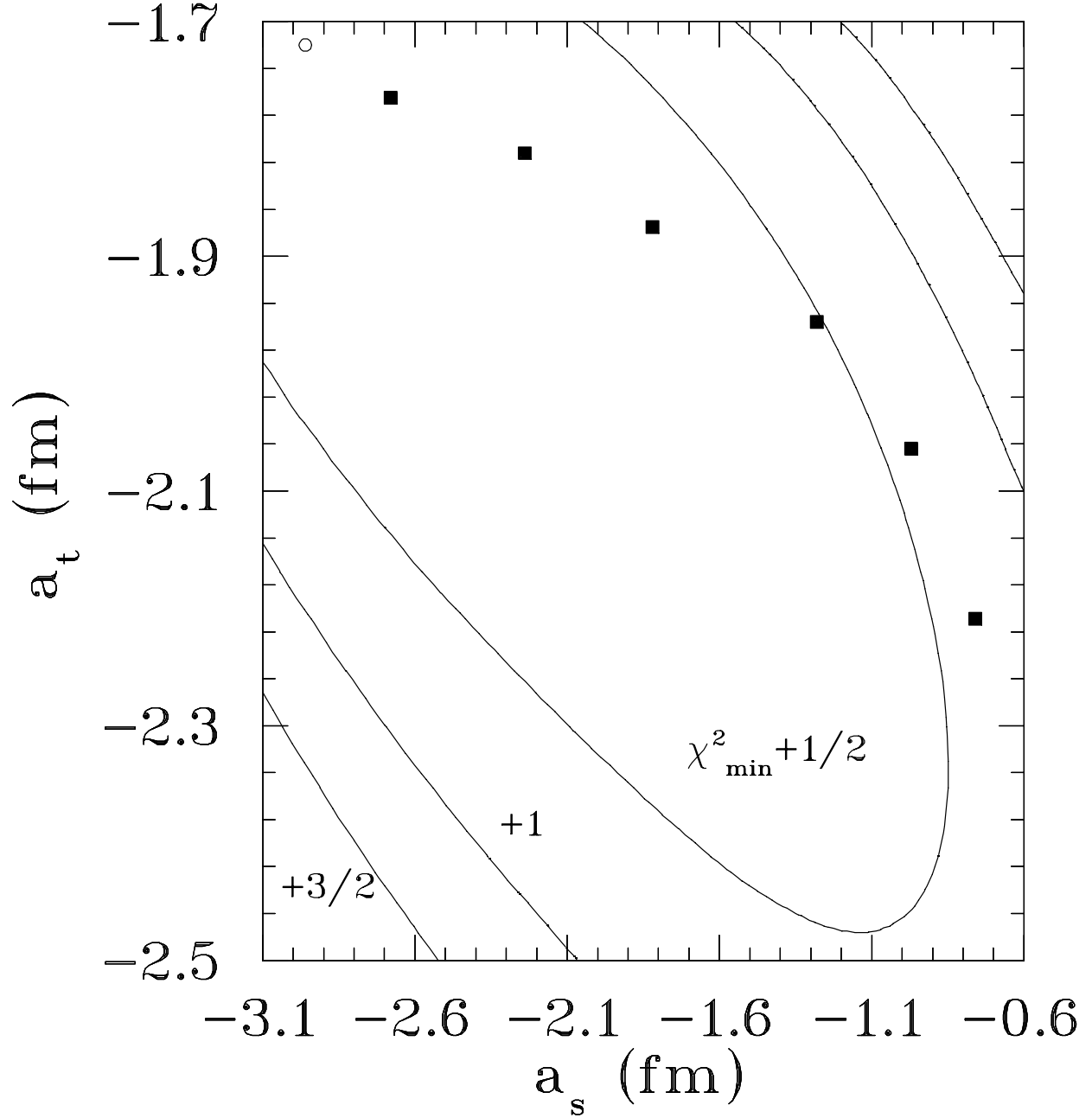


Figure 9: Analysis of the data of Gall *et al.* using the 1 fm scale fits. The contours are lines of constant  $\chi^2$ . Points lying inside the curve labeled +1 are within one standard deviation of the minimum. The solid squares are the values taken for the 6 cases of Ref. [3] and the open circle is the value at the minimum  $\chi^2$  of the fit.



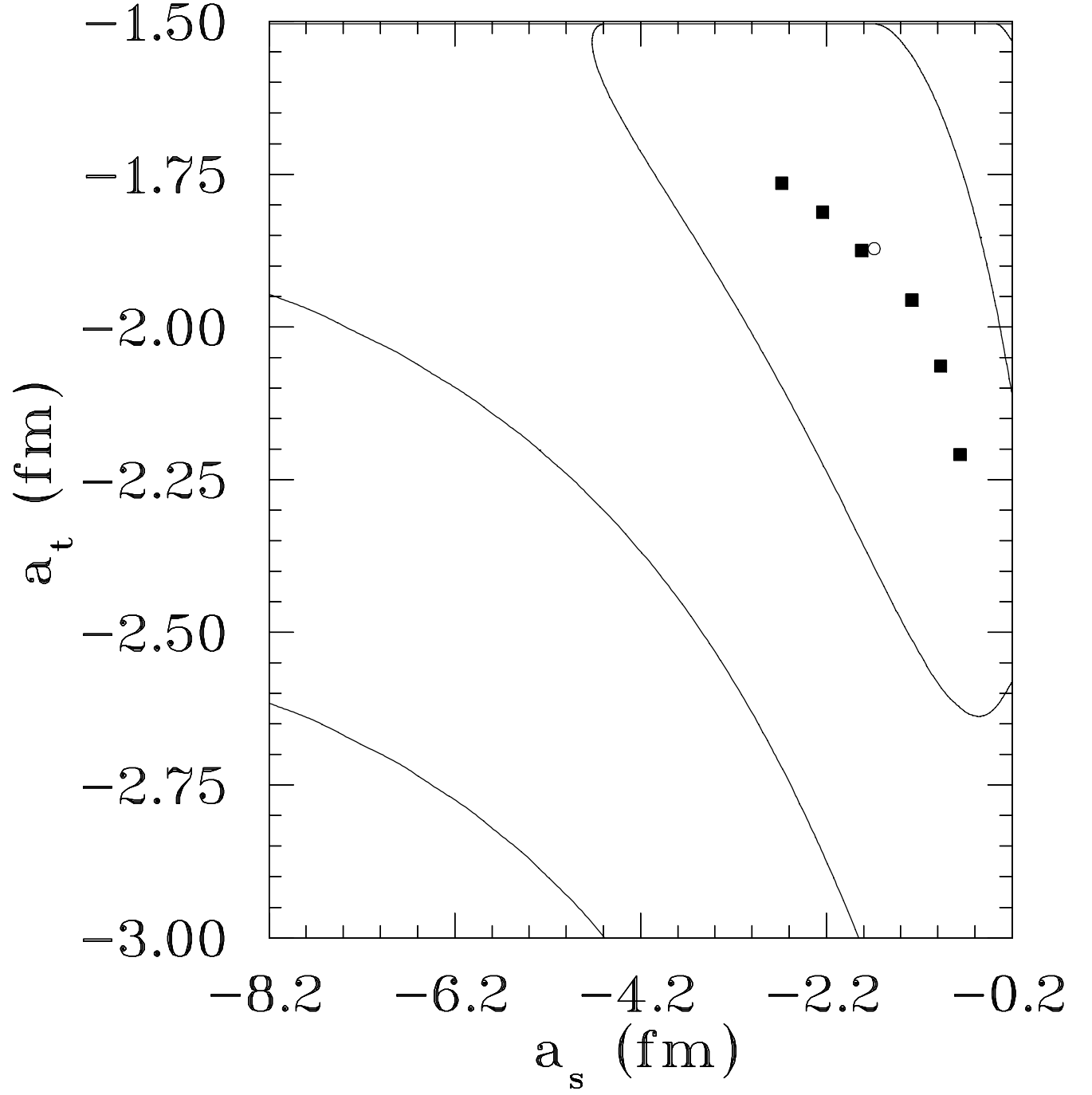


Figure 10: Analysis of the data of Gall *et al.* with the 2 fm range fits. The innermost curve corresponds to one standard deviation, the next to two, etc.

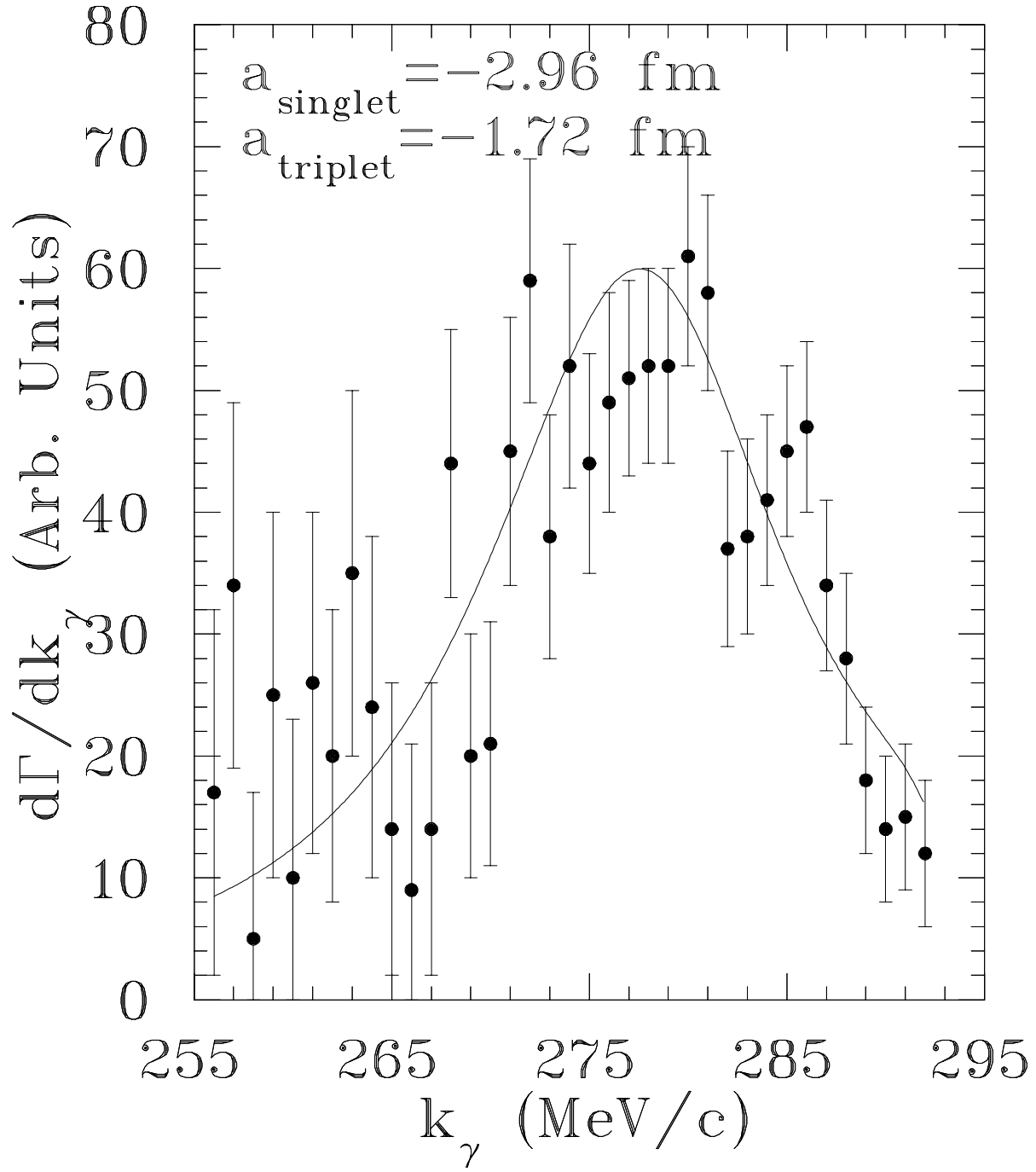


Figure 11: Comparison with the data of Gall *et al.* with the best fit using the 1 fm scale.

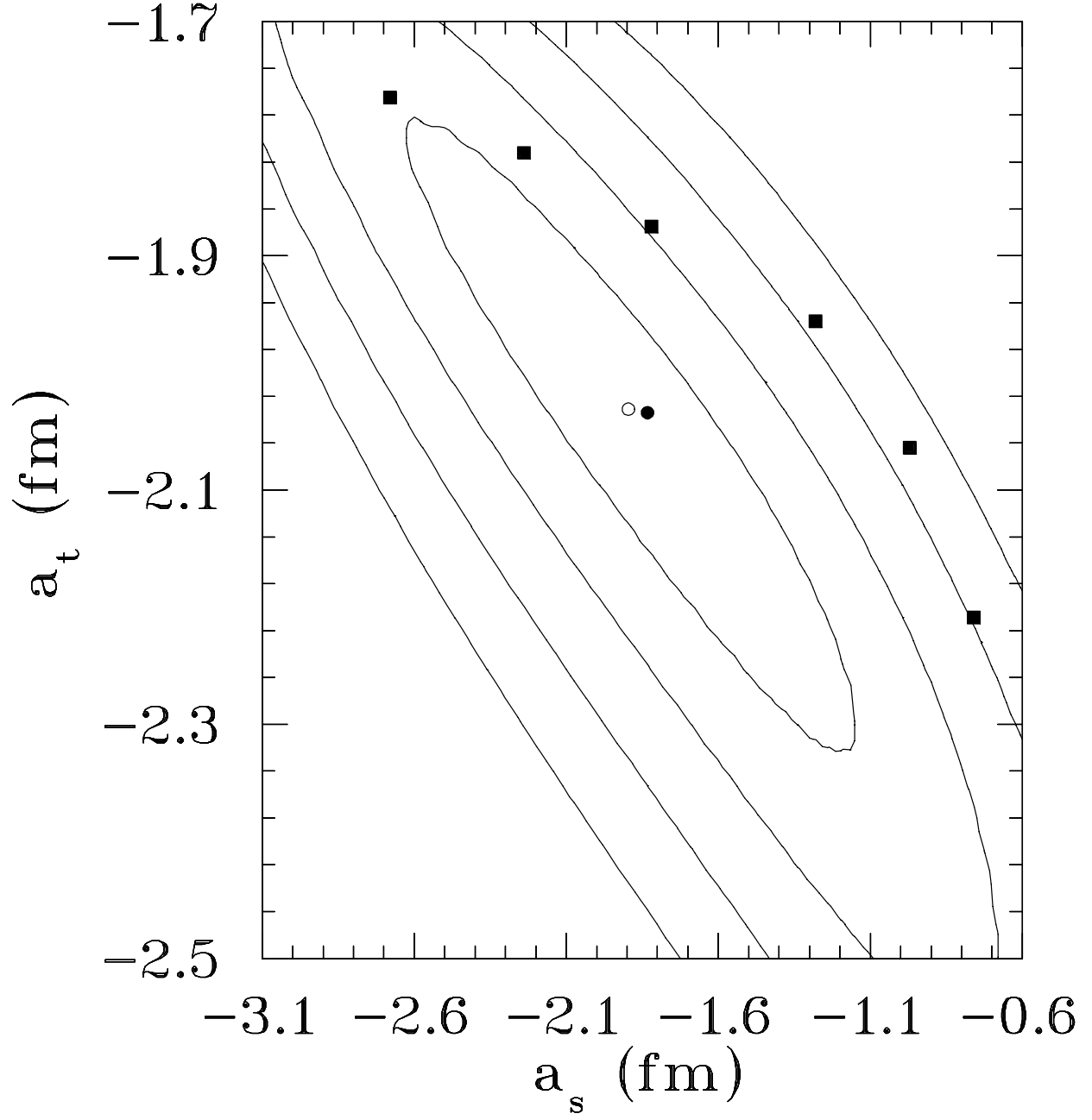


Figure 12: Analysis with a full Jost model of a pseudo data set generated with 3% errors. The 1 fm scale fit was used to generate the data and make the analysis. The solid circle is the input value chosen for the test and the open circle is the central value corresponding to the minimum  $\chi^2$ .

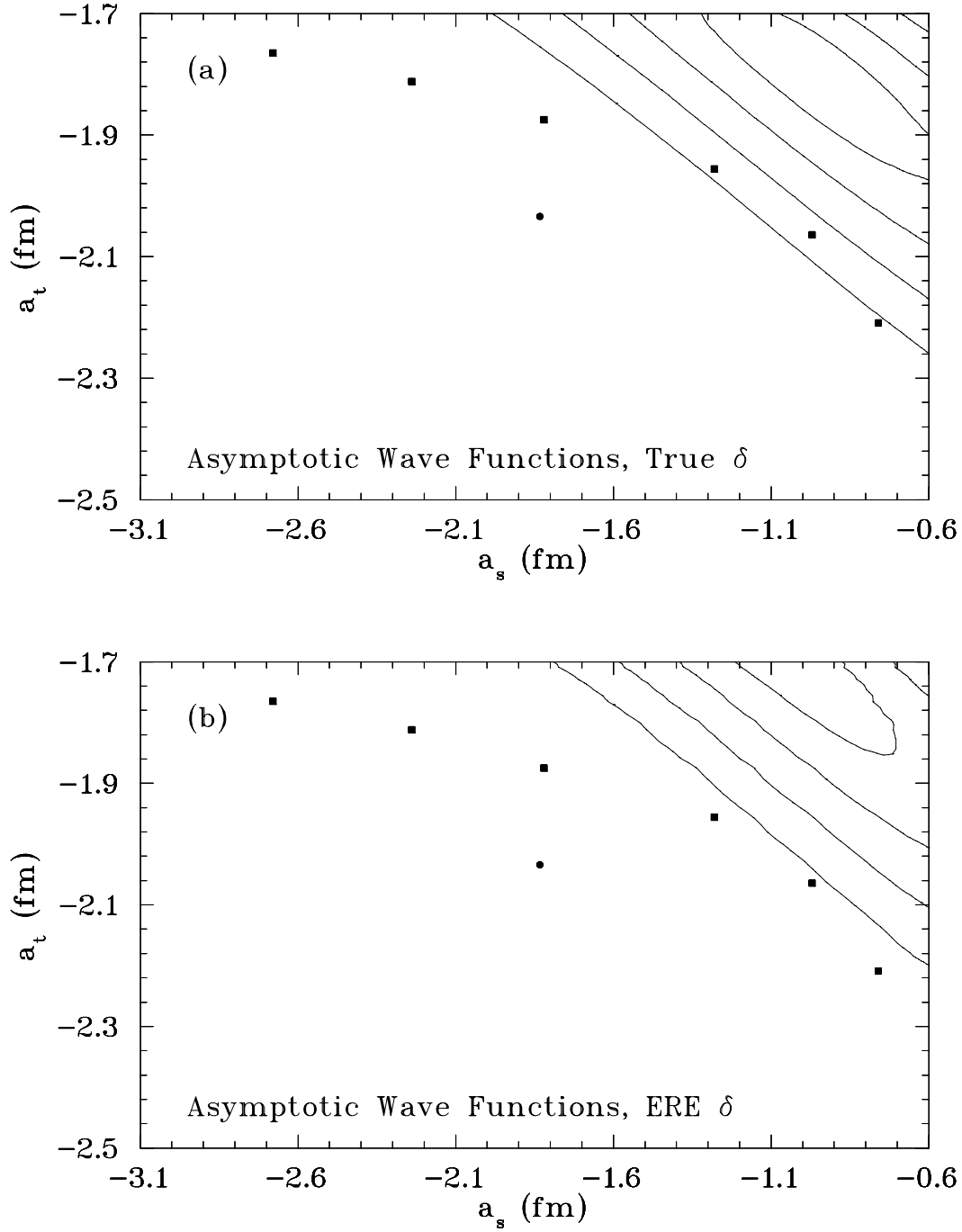


Figure 13: Analysis of the same pseudo data set as in Figure 12 with asymptotic wave functions. In the upper part the correct phase shifts are used while in the lower portion the effective range expansion is used.

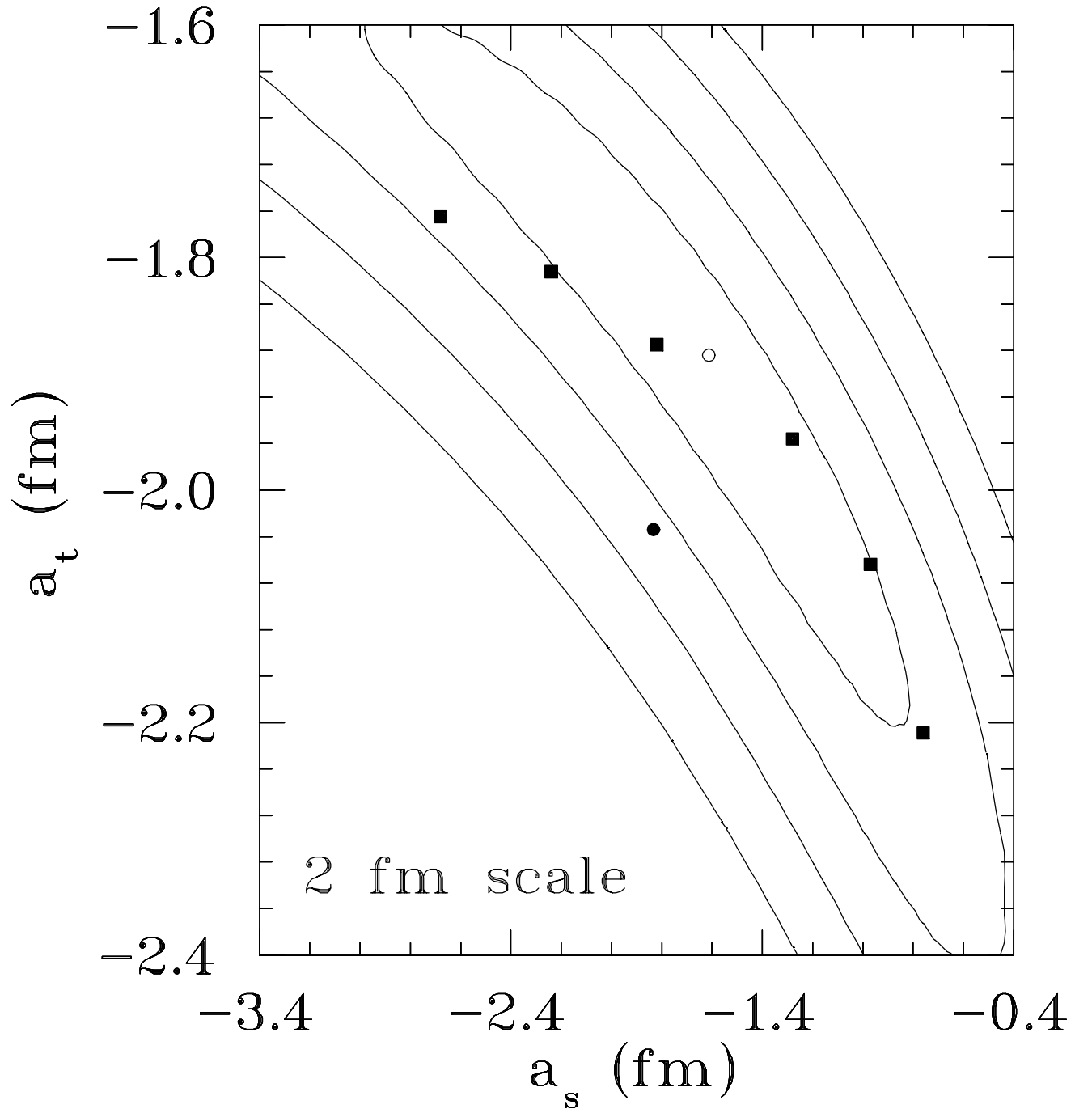


Figure 14: Analysis of the same pseudo data set as in Figure 12 with wave functions generated using the 2 fm range fit.

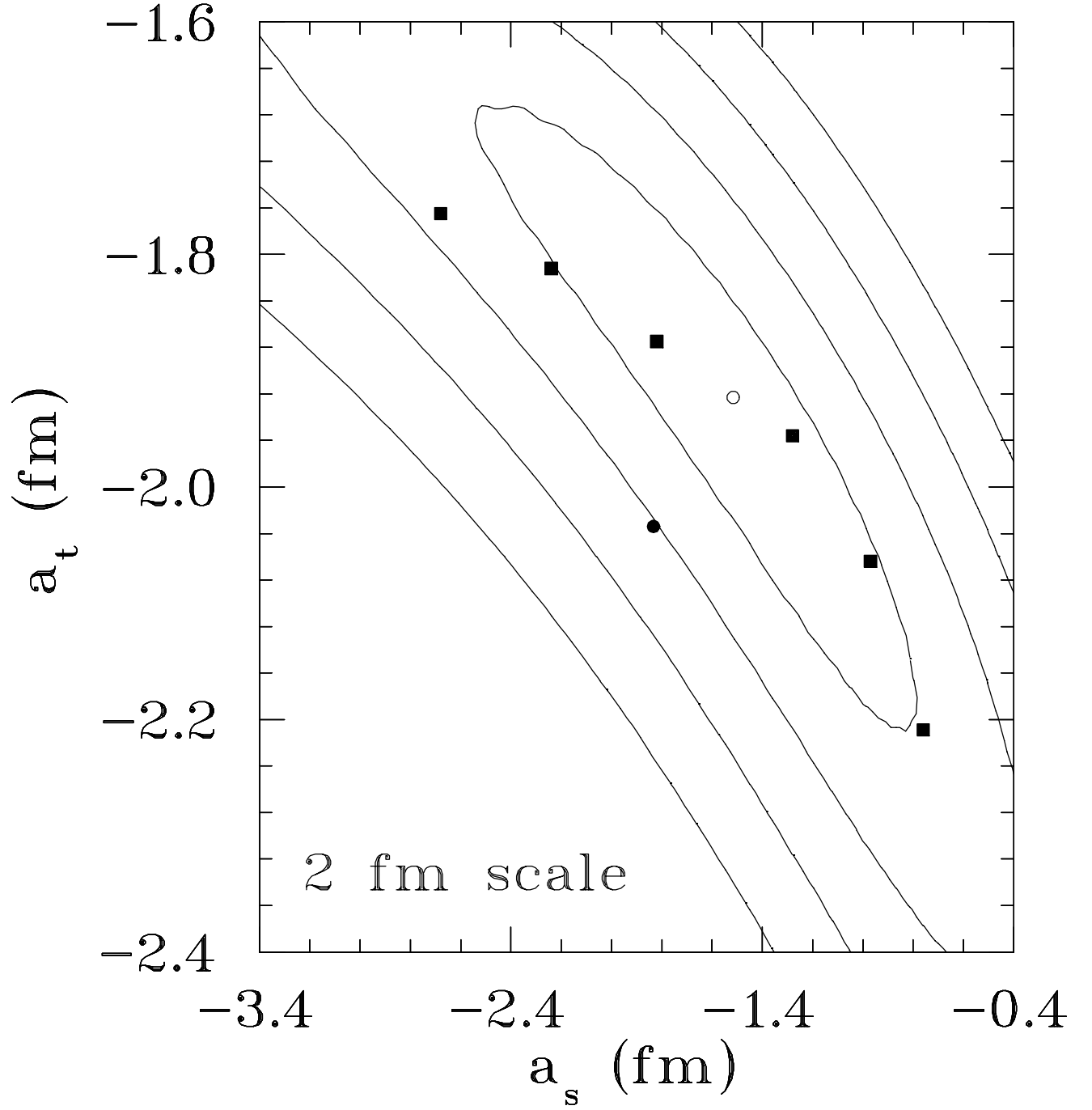


Figure 15: Analysis of the same pseudo data set as in Figure 12 with wave functions using the 2 fm range fit over only the upper 10 MeV of the spectrum.

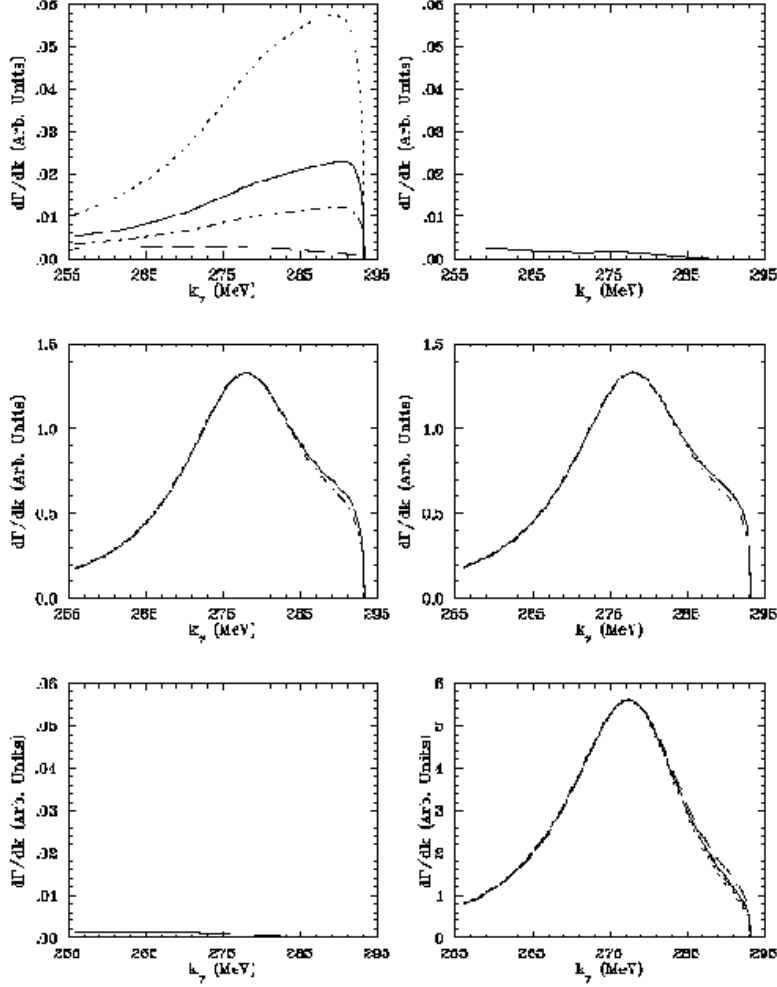


Figure 16: Spectra for the various spin combinations of the initial deuteron and the final photon. The three figures to the left are for right circular polarization and those to the right for left circular polarization of the final photon. The three rows are for  $S_z = +1, 0$  and  $-1$  from the top down. The solid curve has  $a_s = -1.15$ ,  $a_t = -2.06$  the dashed curve  $a_s = -1.96$ ,  $a_t = -2.06$ , the dash-dot curve  $a_s = -1.15$ ,  $a_t = -1.81$  and the dotted curve  $a_s = -0.60$ ,  $a_t = -2.06$  fm.

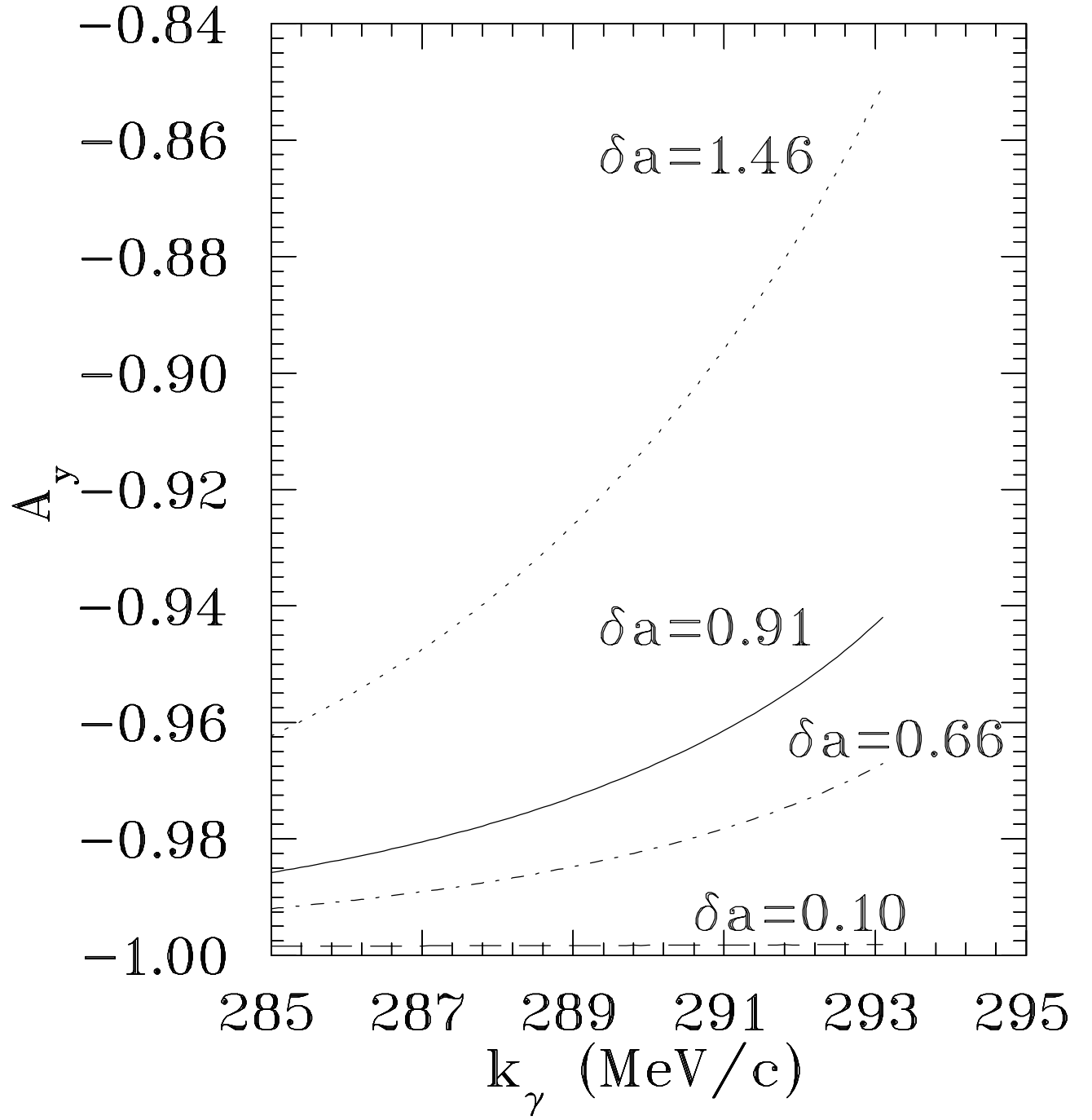


Figure 17: Vector polarization asymmetry for the deuteron initial spins.



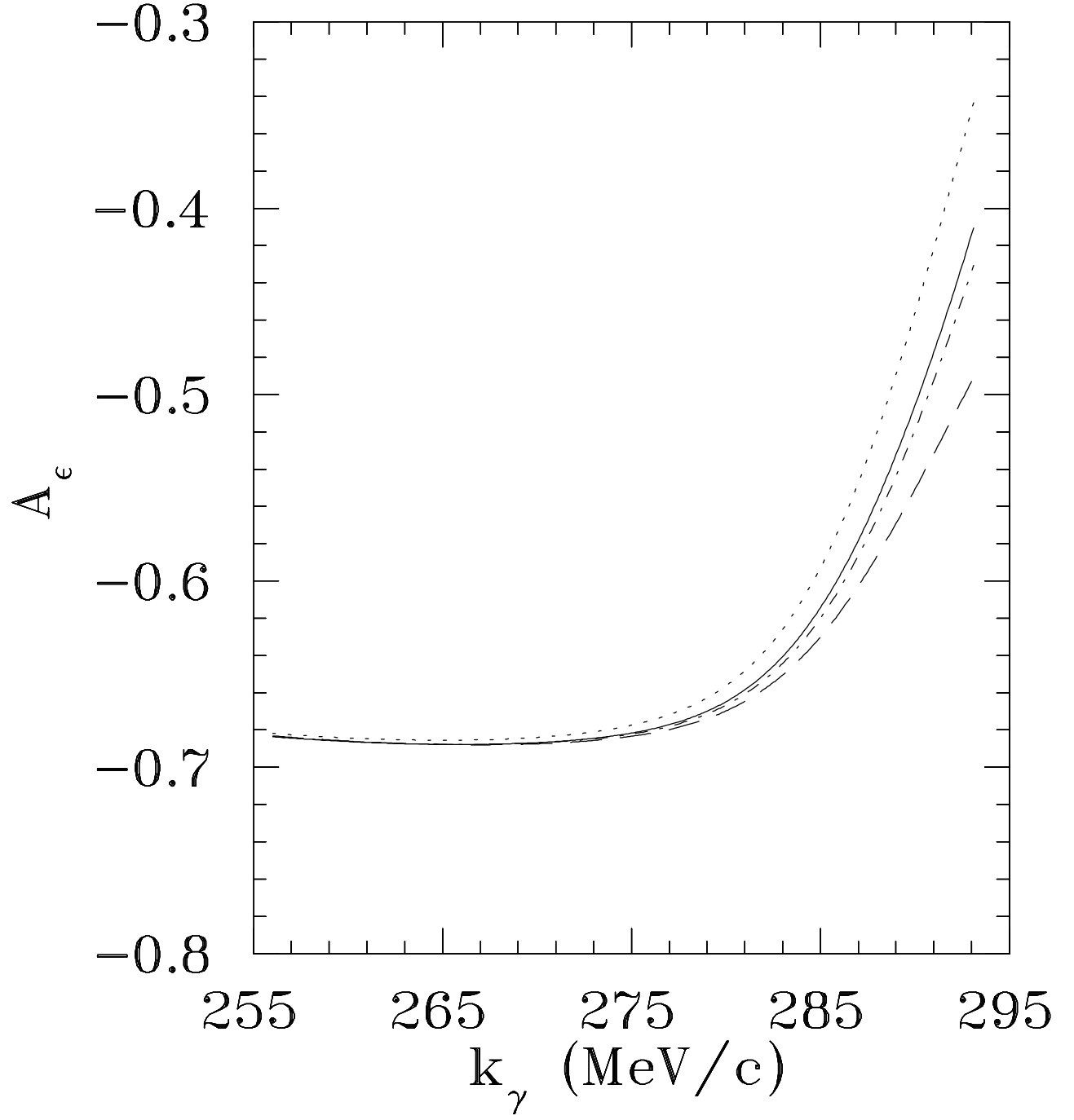


Figure 18: Circular polarization of the photon under the same conditions as the previous figures.